Kinetic Modeling of the CO/H_2O/O_2/NO/SO_2 System: Implications for High-Pressure Fall-off in the $SO_2 + O(+M) = SO_3(+M)$ Reaction

M. A. MUELLER, R. A. YETTER,[1] F. L. DRYER

Department of Mechanical and Aerospace Engineering, Princeton University, Princeton, New Jersey 08544

Received 12 October 1999; accepted 20 January 2000

ABSTRACT: Flow reactor experiments were performed to study moist CO oxidation in the presence of trace quantities of NO (0–400 ppm) and SO_2 (0–1300 ppm) at pressures and temperatures ranging from 0.5–10.0 atm and 950–1040 K, respectively. Reaction profile measurements of CO, CO_2, O_2, NO, NO_2, SO_2, and temperature were used to further develop and validate a detailed chemical kinetic reaction mechanism in a manner consistent with previous studies of the CO/H_2/O_2/NO_X and CO/H_2O/N_2O systems. In particular, the experimental data indicate that the spin-forbidden dissociation-recombination reaction between SO_2 and O-atoms is in the fall-off regime at pressures above 1 atm. The inclusion of a pressure-dependent rate constant for this reaction, using a high-pressure limit determined from modeling the consumption of SO_2 in a N_2O/SO_2/N_2 mixture at 10.0 atm and 1000 K, brings model predictions into much better agreement with experimentally measured CO profiles over the entire pressure range. Kinetic coupling of NO_X and SO_X chemistry via the radical pool significantly reduces the ability of SO_2 to inhibit oxidative processes. Measurements of SO_2 indicate fractional conversions of SO_2 to SO_3 on the order of a few percent, in good agreement with previous measurements at atmospheric pressure. Modeling results suggest that, at low pressures, SO_3 formation occurs primarily through $SO_2 + O(+M) = SO_3(+M)$, but at higher pressures where the fractional conversion of NO to NO_2 increases, SO_3 formation via $SO_2 + NO_2 = SO_3 + NO$ becomes important. For the conditions explored in this study, the primary consumption pathways for SO_3 appear to be $SO_3 + HO_2 = HOSO_2 + O_2$ and $SO_3 + H = SO_2 + OH$. Further study of these reactions would increase the confidence with which model predictions of SO_3 can be viewed. Int J Chem Kinet 32: 317–339, 2000

Correspondence to: Frederick L. Dryer
Contract grant sponsor: NASA Glenn Research Center
Contract grant number: NAG3–1587 and NAG3–2164
[1]Present address: Department of Mechanical and Nuclear Engineering, Pennsylvania State University, University Park, PA 16802

INTRODUCTION

The combustion of sulfur–bearing fuels almost always yields sulfur dioxide as the predominant sulfur-containing product [1]. Flame studies [2,3] have shown that SO_2 catalyzes the recombination of radicals, leading to lower flame speeds and more rapid relaxation of super-equilibrium radical levels. Under fuel-lean conditions, a small percentage of the SO_2 is typically oxidized to SO_3, which, at low temperatures, readily reacts with water to form sulfuric acid. In industrial power plants, this conversion of fuel sulfur to S(VI) (SO_3 and H_2SO_4) leads to the deposition of corrosive condensates that adversely affect efficiency and durability [4]. Aircraft emissions of S(VI) have also received considerable interest as these species apparently serve as important precursors to sulfate aerosols [5]. In the upper atmosphere, these aerosols contribute to the formation of persistent contrails and perturb chemical processes by providing surface area for heterogeneous chemistry [6,7]. One-dimensional simulations [8] of postcombustor gases flowing through turbine and exhaust nozzles indicate that 2–10% of aircraft sulfur emissions may exist as S(VI), with the principal component being SO_3. These calculations further indicate that SO_3 formation is kinetically limited and that competition for radicals between CO_X, NO_X, and SO_X species influences the SO_3/SO_2 ratio. Similar interactions via the radical pool as well as direct interactions between nitrogen and sulfur-containing species appear to explain the effects of sulfur addition on combustion-generated NO [9,10].

A number of recent studies have investigated the kinetic interactions between NO and moist CO chemistry [11,12,13]. In reference [13], we provide a $CO/H_2/O_2/NO_X$ reaction mechanism which well predicts the oxidation of H_2 and CO in the presence of small concentrations of NO and NO_2 at pressures and temperatures ranging from 0.4–14.0 atm and 750–1100 K, respectively. The combustion kinetics of sulfur compounds and potential interactions with fuel oxidative processes are comparatively less understood. The review articles of Hynes and Wine [14] and Cullis and Mulcahy [15] summarize the basic chemistry of sulfur in combustion systems. Experimental and modeling studies in flames [2,3], shock tubes [16], and flow reactors [17] have identified important reaction pathways and provide estimates of rate constants where elementary rate data are not available. Of particular interest to the present work, the flow reactor study of Glarborg et al. [17] investigated the effects of SO_2 and NO on moist CO oxidation at atmospheric pressure and temperatures between 800–1300 K. SO_2 was found to inhibit CO oxidation primarily through the scavenging of O-atoms via

$$SO_2 + O\ (+M) = SO_3\ (+M), \qquad (129)$$

where the implication of high-pressure fall-off behavior has been added here. The observed inhibition due to SO_2 was significantly reduced through the addition of NO, an effect not understood in the context of their reaction mechanism.

As we have shown previously for NO_X [13] and CH_4 [18,19], kinetic interactions between perturbing species and the $CO/H_2O/O_2$ system are highly pressure sensitive due to compositional changes in the radical pool. In addition, important radical recombination reactions are in the fall-off region between their low- and high-pressure limits at pressures and temperatures relevant for practical combustion applications. The present study builds upon our previous work and that of Glarborg et al. [17] by investigating the oxidation of CO in the presence of NO and SO_2 at pressures and temperatures ranging from 0.5–10.0 atm and 950–1040 K, respectively. Reactivity trace data at fixed residence time and varying SO_2 are used to phenomenologically describe the perturbing effects of SO_2 in the presence of NO. Reaction profile measurements of CO, CO_2, O_2, NO, NO_2, SO_2, and temperature as functions of time are used to constrain the development a $CO/H_2O/O_2/NO_X/SO_X$ reaction mechanism previously validated for the $CO/H_2/O_2/NO_X$ system.

FLOW REACTOR EXPERIMENT

The experimental apparatus used in this study is a variable-pressure (0.2–20 atm) turbulent flow reactor capable of operating to temperatures approaching 1200 K. The design and operating characteristics of this reactor have been discussed in detail elsewhere [20] and a schematic is provided in reference [21]. Carrier gas (typically N_2) is heated by an electric resistant heater and mixed with oxygen as it enters a 10.2-cm-diameter quartz duct that serves as the test section. The remaining reactants are diluted with inert and are rapidly mixed with the carrier gas at the entrance to a silica foam diffuser. The reacting mixture is sampled at axial positions downstream of the diffuser using a hot-water-cooled, stainless steel sampling probe, which continuously extracts and convectively quenches a small percentage of the flow. The sampled gas flows via heated teflon lines to a series of analytical equipment including a Fourier transform infrared (FTIR) spectrometer (Nicolet Model 560), an electrochemical

O_2 analyzer (Infrared Industries Model 2200), and nondispersive CO and CO_2 analyzers (Horiba Model PIR 2000). The uncertainties in the measurements reported here are: H_2O, ±5%; O_2, ±4%; CO, ±3%; CO_2, ±3%; NO, ±5%; NO_2, ±5%; and SO_2, ±3% of reading. Minimum uncertainties in the NO, NO_2, and SO_2 readings are estimated to be ±2 ppm. At low temperatures, SO_3 reacts rapidly with H_2O to form H_2SO_4; therefore, SO_3 cannot be measured using the gas sampling technique employed here. Measurements of SO_2, on the other hand, are not significantly affected by the presence of H_2O. In nonreacting experiments with known SO_2 mole fractions in 0.75% O_2/0.5% H_2O/N_2 mixtures at 950 K, we found less than 1% disappearance of SO_2. Model predictions of the $CO/H_2O/O_2/NO/SO_2$ reaction at the conditions considered here indicate that SO_3 mole fractions are approximately an order of magnitude larger than those of any other sulfur-containing species, with the exception of SO_2. Therefore, SO_3 mole fractions can be reasonably inferred from the measured consumption of SO_2. The temperature of the reacting mixture is measured at the sampling location with a silica-coated type-R thermocouple accurate to approximately ±3 K.

The observed reaction time is varied by positioning the fuel injector with respect to the fixed sampling location. Dilute mixtures limit heat release and maintaining the wall temperature at the initial gas temperature approximates adiabatic operation. High convective velocities in the test section suppress spatial gradients and permit neglect of the diffusive terms in the governing equations. Neglecting these terms leads to a simple initial value, quasi-steady reacting flow problem in which distance and time can be interchanged. Thus, the experiment can therefore be modeled as a zero-dimensional system using SENKIN [22] with isobaric and adiabatic approximations. Because the model assumes that the reactants are instantaneously mixed, predicted induction times are typically not relevant to those observed in our experiments, where short-lived nonhomogeneities perturb the initial growth of the radical pool. Similar perturbations may be caused by very low concentrations of impurities in the reactants. However, the underlying kinetics after the induction period are sufficiently fast to allow for rapid adjustment of the radical pool to local conditions thereafter. Under these circumstances, Yetter et al. [23] showed that such perturbations affect only the chemical induction times and not the reaction gradients in the postinduction region where measurements are made. Although absolute timescales may be perturbed, relative timescales in the postinduction reaction are accurate. Thus, unless otherwise noted, comparisons between reaction profile data and model predictions are facilitated by shifting the experimental data in absolute time to agree with model predictions at some convenient time, in this case, the point of 50% fuel consumption.

REACTION MECHANISM

The kinetic model builds hierarchically upon a previously developed $CO/H_2/O_2/NO_X$ kinetic mechanism to include the species and reactions important to describing SO_X interactions. The $CO/H_2O/O_2$ submechanism is derived from the reaction mechanism of Kim et al. [24] but incorporates important modifications from references [13,21]. As discussed in reference [13], the reactions involving nitrogen oxides are taken primarily from the $CO/H_2O/N_2O$ mechanism of Allen et al. [25] and the chemical kinetic database of Tsang and Herron [26]. Reactions involving sulfur-containing species are extracted from the work of Glarborg et al. [17] with modifications as noted below. Details of the reaction mechanism are given in Table I. The elementary reactions are numbered in a manner consistent with references [13,25], and we include only those reactions relevant to the present study. A more comprehensive reaction mechanism can be assembled by adding reactions (31)–(38) and (67)–(125) from Allen et al. and the H_XS subset of reactions from Glarborg et al. In the following, reaction numbers followed by the letter "R" denote that the reaction is written in the reverse direction as provided in Table I. All thermochemical data are taken from Kee et al. [27] except those data for HSO, HOS, HOSH, H_2SO, HOSO, HSO_2, HOSHO, and $HOSO_2$, which are from Glarborg et al., and the heat of formation for HO_2, which is from Hill and Howard [28].

The elementary rate constants for the sulfur chemistry are taken from direct measurements when available and are supplemented with semiempirical calculations for reactions involving the HSO_2/HOSO, HSOH/H_2SO, and $HOSO_2$ complexes. The rate constants provided by Glarborg et al. [17] for these latter reactions are QRRK estimates at 1 atm for temperatures between 300–1500 K. Details of these calculations and additional rate parameters at other pressures are provided in reference [29]. We have modified several rate constants within the sulfur submechanism to incorporate pressure-dependent behavior in reactions involving the combination of SO_2 and/or SO_3 with H, O, and OH radicals. Most importantly, our experimental data and modeling results clearly indicate that the spin-forbidden dissociation-recombination reaction

Table I Detailed Reaction Mechanism Units are cm^3-mole-sec-cal-K; $k = AT^n \exp(-E_a/RT)$

#	Reaction	A	n	E_a	Ref.
H_2–O_2 Chain Reactions					
1.	$H + O_2 = O + OH$	1.91×10^{14}	0.00	1.64×10^{4}	[53]
2.	$O + H_2 = H + OH$	5.08×10^{04}	2.67	6.29×10^{3}	[54]
3.	$OH + H_2 = H_2O + H$	2.16×10^{08}	1.51	3.43×10^{3}	[55]
4.	$H_2O + O = OH + OH$	2.97×10^{06}	2.02	1.34×10^{4}	[56]
H_2–O_2 Dissociation/Recombination Reactions					
5.	$H_2 + M = H + H + M$[a]	4.58×10^{19}	−1.40	1.04×10^{5}	[57]
	$H_2 + Ar = H + H + Ar$	5.84×10^{18}	−1.10	1.04×10^{5}	[57]
6	$O + O + M = O_2 + M$[a]	6.16×10^{15}	−0.50	0.00	[57]
	$O + O + Ar = O_2 + Ar$	1.89×10^{13}	0.00	-1.79×10^{3}	[57]
7.	$H + O + M = OH + M$[a]	4.71×10^{18}	−1.00	0.00	[57]
8.	$OH + H + M = H_2O + M$[a]	2.21×10^{22}	−2.00	0.00	[57]
	$OH + H + Ar = H_2O + Ar$	8.41×10^{21}	−2.00	0.00	[57]
Formation and Consumption of HO_2					
9.	$H + O_2 + M = HO_2 + M$[a]	3.50×10^{16}	−0.41	-1.12×10^{3}	[58]
	$H + O_2 + Ar = HO_2 + Ar$	1.49×10^{15}	0.00	-1.00×10^{3}	[59]
	$H + O_2 = HO_2$ ($F_C^{N2} = 0.5$; $F_C^{Ar} = 0.45$)[b]	1.48×10^{12}	0.60	0.00	[60]
10.	$HO_2 + H = H_2 + O_2$	1.66×10^{13}	0.00	8.20×10^{2}	[21]
11.	$HO_2 + H = OH + OH$	7.08×10^{13}	0.00	3.00×10^{2}	[21]
12.	$HO_2 + O = O_2 + OH$	3.25×10^{13}	0.00	0.00	[61]
13.	$HO_2 + OH = H_2O + O_2$	2.89×10^{13}	0.00	-5.00×10^{2}	[61]
Formation and Consumption of H_2O_2					
14.[c]	$HO_2 + HO_2 = H_2O_2 + O_2$	4.20×10^{14}	0.00	1.20×10^{4}	[62]
	$HO_2 + HO_2 = H_2O_2 + O_2$	1.30×10^{11}	0.00	-1.63×10^{3}	[62]
15.	$H_2O_2 + M = OH + OH + M$[a]	1.20×10^{17}	0.00	4.55×10^{4}	[63]
	$H_2O_2 + Ar = OH + OH + Ar$	1.90×10^{16}	0.00	4.30×10^{4}	[64]
	$H_2O_2 = OH + OH$ ($F_C = 0.5$)[b]	2.95×10^{14}	0.00	4.84×10^{4}	[64]
16.	$H_2O_2 + H = H_2O + OH$	2.41×10^{13}	0.00	3.97×10^{3}	[57]
17.	$H_2O_2 + H = HO_2 + H_2$	4.82×10^{13}	0.00	7.95×10^{3}	[57]
18.	$H_2O_2 + O = OH + HO_2$	9.55×10^{06}	2.00	3.97×10^{3}	[57]
19.[c]	$H_2O_2 + OH = H_2O + HO_2$	1.00×10^{12}	0.00	0.00	[65]
	$H_2O_2 + OH = H_2O + HO_2$	5.80×10^{14}	0.00	9.56×10^{3}	[65]
NO Reactions					
20.	$NO + O + M = NO_2 + M$[a]	4.72×10^{24}	−2.87	1.55×10^{3}	[26]
	$NO + O + Ar = NO_2 + Ar$	7.56×10^{19}	−1.41	0.00	[66]
	$NO + O = NO_2$ ($F_C = 0.95 - 1.0 \times 10^{-4}$ T)[b]	3.00×10^{13}	0.00	0.00	[67]
21.	$NO + H + M = HNO + M$[d]	5.00×10^{19}	−1.32	7.35×10^{2}	[68]
	$NO + H = HNO$ ($F_C = 0.82$)[b]	1.52×10^{15}	−0.41	0.00	[26]
22.	$NO + OH + M = HONO + M$[d]	5.08×10^{23}	−2.51	-6.76×10^{1}	[26]
	$NO + OH = HONO$ ($F_C = 0.62$)[b]	1.99×10^{12}	−0.05	-7.21×10^{2}	[69]
NO_2 Reactions					
23.	$NO_2 + H_2 = HONO + H$	1.30×10^{04}	2.76	1.50×10^{4}	[70]
24.	$NO_2 + O = O_2 + NO$	1.05×10^{14}	−0.52	0.00	[71]
25.	$NO_2 + O + M = NO_3 + M$[d]	1.49×10^{28}	−4.08	2.47×10^{3}	[26]
	$NO_2 + O = NO_3$ ($F_C = 0.79 - 1.8 \times 10^{-4}$ T)[b]	1.33×10^{13}	0.00	0.00	[26]
26.	$NO_2 + H = NO + OH$	1.32×10^{14}	0.00	3.62×10^{2}	[72]
27.	$NO_2 + OH + M = HNO_3 + M$[d]	6.42×10^{32}	−5.49	2.35×10^{3}	[26]
	$NO_2 + OH = HNO_3$ ($F_C = 0.73 - 2.5 \times 10^{-4}$ T)[b]	4.52×10^{13}	0.00	0.00	[69]
28.	$NO + HO_2 = NO_2 + OH$	2.11×10^{12}	0.00	-4.79×10^{2}	[26]
29.	$NO_2 + NO_2 = NO_3 + NO$	9.64×10^{09}	0.73	2.09×10^{4}	[26]
30.	$NO_2 + NO_2 = 2NO + O_2$	1.63×10^{12}	0.00	2.61×10^{4}	[26]
NH Reactions					See Allen et al. [25]
HNO Reactions					
39.	$HNO + H = NO + H_2$	4.40×10^{11}	0.72	6.50×10^{2}	[73]
40.	$HNO + O = OH + NO$	1.81×10^{13}	0.00	0.00	[26]

(Continued)

Table I (Continued)

#	Reaction	A	n	E_a	Ref.
41.	$HNO + OH = H_2O + NO$	1.30×10^{07}	1.88	-9.56×10^{2}	[74]
42.	$HNO + NO = N_2O + OH$	2.00×10^{12}	0.00	2.60×10^{4}	[75]
43.	$HNO + NO_2 = HONO + NO$	6.02×10^{11}	0.00	1.99×10^{3}	[26]
44.	$HNO + HNO = H_2O + N_2O$	8.51×10^{08}	0.00	3.08×10^{3}	[76]
HONO Reactions					
45.	$HONO + O = OH + NO_2$	1.20×10^{13}	0.00	5.96×10^{3}	[26]
46.	$HONO + OH = H_2O + NO_2$	1.70×10^{12}	0.00	-5.20×10^{2}	[77]
N_2O Reactions					
47.	$N_2O + M = N_2 + O + M$[e]	9.13×10^{14}	0.00	5.77×10^{4}	[20]
	$NO_2 = N_2 + O \quad (F_C = 1.0)$[b]	7.91×10^{10}	0.00	5.60×10^{4}	[20]
48.	$N_2O + O = O_2 + N_2$	1.00×10^{14}	0.00	2.80×10^{4}	[59]
49.	$N_2O + O = NO + NO$	1.00×10^{14}	0.00	2.80×10^{4}	[59]
50.[c]	$N_2O + H = N_2 + OH$	2.53×10^{10}	0.00	4.55×10^{3}	[78]
	$N_2O + H = N_2 + OH$	2.23×10^{14}	0.00	1.68×10^{4}	[78]
51.	$N_2O + OH = HO_2 + N_2$	2.00×10^{12}	0.00	4.00×10^{4}	[79]
52.	$N_2O + NO = NO_2 + N_2$	1.00×10^{14}	0.00	4.97×10^{4}	[80]
CO Reactions					
53.	$CO + O + M = CO_2 + M$[a]	1.35×10^{24}	-2.79	4.19×10^{3}	[81]
	$CO + O = CO_2 \quad (F_C = 1.0)$[b]	1.80×10^{10}	0.00	2.83×10^{3}	[82]
54.	$CO + O_2 = CO_2 + O$	2.53×10^{12}	0.00	4.77×10^{4}	[57]
55.	$CO + OH = CO_2 + H$	1.40×10^{05}	1.95	-1.35×10^{3}	[83]
56.	$CO + HO_2 = CO_2 + OH$	3.01×10^{13}	0.00	2.30×10^{4}	[21]
57.	$CO + N_2O = CO_2 + N_2$	5.01×10^{13}	0.00	4.40×10^{4}	[84]
58.	$CO + NO_2 = CO_2 + NO$	9.03×10^{13}	0.00	3.38×10^{4}	[26]
HCO Reactions					
59.	$HCO + M = H + CO + M$[f]	1.85×10^{17}	-1.00	1.70×10^{4}	[85]
60.	$HCO + O_2 = CO + HO_2$	7.58×10^{12}	0.00	4.06×10^{2}	[86]
61.	$HCO + H = CO + H_2$	7.23×10^{13}	0.00	0.00	[87]
62.	$HCO + O = CO + OH$	3.00×10^{13}	0.00	0.00	[57]
63.	$HCO + OH = CO + H_2O$	3.00×10^{13}	0.00	0.00	[57]
64.	$HCO + NO = HNO + CO$	7.23×10^{12}	0.00	0.00	[26]
65.	$HCO + NO_2 = CO + HONO$	1.24×10^{23}	-3.29	2.35×10^{3}	[88]
66.	$HCO + NO_2 = H + CO_2 + NO$	8.39×10^{15}	-0.75	1.93×10^{3}	[88]
NH_2, NH_3, NNH, N_2H_X Reactions					See Allen et al. [25]
SO_X Reactions					
126.	$SO_3 + H = HOSO + O$	2.5×10^{05}	2.92	5.03×10^{4}	[17]
127.	$SO_3 + O = SO_2 + O_2$	4.4×10^{11}	0.00	6.10×10^{3}	[2]
128.	$SO_3 + SO = SO_2 + SO_2$	1.0×10^{12}	0.00	4.00×10^{3}	[89]
129.	$SO_2 + O + M = SO_3 + M$[g]	4.0×10^{28}	-4.00	5.25×10^{3}	[30]
	$SO_2 + O = SO_3 \quad (F_C = 1.0)$[b]	9.2×10^{10}	0.00	2.38×10^{3}	this work
130.	$SO_2 + OH + M = HOSO_2 + M$	4.5×10^{25}	-3.30	7.15×10^{2}	[31]
	$SO_2 + OH = HOSO_2 \quad (F_C = 0.29 + 0.64 \exp(-T/300))$[b]	7.2×10^{12}	0.00	7.15×10^{2}	[31]
131.	$SO_2 + OH = HOSO + O$	3.9×10^{08}	1.89	7.60×10^{4}	[17]
132.	$SO_2 + OH = SO_3 + H$	4.9×10^{02}	2.69	2.38×10^{4}	[17]
133.	$SO_2 + CO = SO + CO_2$	2.7×10^{12}	0.00	4.38×10^{4}	[90]
134.	$SO + M = S + O + M$	4.0×10^{14}	0.00	1.07×10^{5}	[91]
135.	$SO + H + M = HSO + M$	5.0×10^{15}	0.00	0.00	[17]
136.	$SO + O + M = SO_2 + M$[g]	2.9×10^{24}	-2.90	0.00	[32]
	$SO + O = SO_2 \quad (F_C = 0.55)$[b]	3.2×10^{13}	0.00	0.00	[33]
137.	$SO + OH = SO_2 + H$	5.2×10^{13}	0.00	0.00	[92]
138.	$SO + OH + M = HOSO + M$	8.0×10^{21}	-2.16	8.30×10^{2}	[17]
139.	$SO + O_2 = SO_2 + O$	6.2×10^{03}	2.42	3.05×10^{3}	[40,93]
140.	$SO + SO = SO_2 + S$	2.0×10^{12}	0.00	4.00×10^{3}	[94]
HS_XO_Y Reactions					
141.	$HSO + H = HSOH$	2.5×10^{20}	-3.14	9.20×10^{2}	[17]

(Continued)

Table I (Continued)

#	Reaction	A	n	E_a	Ref.
142.	$HSO + H = SH + OH$	4.9×10^{19}	−1.86	1.56×10^{3}	[17]
143.	$HSO + H = S + H_2O$	1.6×10^{09}	1.37	-3.40×10^{2}	[17]
144.	$HSO + H = H_2SO$	1.8×10^{17}	−2.47	5.00×10^{1}	[17]
145.	$HSO + H = H_2S + O$	1.1×10^{06}	1.03	1.04×10^{4}	[17]
146.	$HSO + H = SO + H_2$	1.0×10^{12}	0.00	0.00	[17]
147.	$HSO + O = SO_2 + H$	4.5×10^{14}	−0.40	0.00	[17]
148.	$HSO + O = HOS + O$	4.8×10^{08}	1.02	5.34×10^{3}	[17]
149.	$HSO + O = SO + OH$	1.4×10^{13}	0.15	3.00×10^{2}	[17]
150.	$HSO + O + M = HOSO + M$	6.9×10^{19}	−1.61	1.59×10^{3}	[17]
151.	$HSO + O + M = HSO_2 + M$	1.1×10^{19}	−1.73	-5.00×10^{1}	[17]
152.	$HSO + OH = HOSHO$	5.2×10^{28}	−5.44	3.17×10^{3}	[17]
153.	$HSO + OH = HOSO + H$	5.3×10^{07}	1.57	3.75×10^{3}	[17]
154.	$HSO + OH = SO + H_2O$	1.7×10^{09}	1.03	4.07×10^{2}	[17]
155.	$HSO + O_2 = SO_2 + OH$	1.0×10^{12}	0.00	0.00	[17]
156.	$HSOH = SH + OH$	2.8×10^{39}	−8.75	7.52×10^{4}	[17]
157.	$HSOH = S + H_2O$	5.8×10^{29}	−5.60	5.45×10^{4}	[17]
158.	$HSOH = H_2S + O$	9.8×10^{16}	−3.40	8.65×10^{4}	[17]
159.	$H_2SO = H_2S + O$	4.9×10^{28}	−6.66	7.17×10^{4}	[17]
160.	$HOSO + M = HOS + O + M$	2.5×10^{30}	−4.80	1.19×10^{5}	[17]
161.	$HOSO + M = SO_2 + H + M$	1.6×10^{31}	−4.53	4.92×10^{4}	[38]
	$HOSO = SO_2 + H \quad (F_C = 0.45)$[b]	1.7×10^{10}	0.80	4.69×10^{4}	[38]
162.	$HOSO + H = SO + H_2O$	6.3×10^{-10}	6.29	-1.90×10^{3}	[17]
163.	$HOSO + OH = SO_2 + H_2O$	1.0×10^{12}	0.00	0.00	[17]
164.	$HOSO + O_2 = SO_2 + HO_2$	1.0×10^{12}	0.00	1.00×10^{3}	[40]
165.	$HSO_2 + M = SO_2 + H + M$	3.5×10^{25}	−3.29	1.91×10^{4}	[38]
	$HSO_2 = SO_2 + H \quad (F_C = 1.0)$[b]	2.0×10^{11}	−0.90	1.84×10^{4}	[38]
166.	$HSO_2 + M = HOSO + M$	1.7×10^{35}	−5.64	5.54×10^{4}	[38]
	$HSO_2 = HOSO \quad (F_C = 0.44)$[b]	1.0×10^{9}	1.03	5.00×10^{4}	[38]
167.	$HOSO_2 = HOSO + O$	5.4×10^{18}	−2.34	1.06×10^{5}	[17]
168.	$HOSO_2 + M = SO_3 + H + M$	3.2×10^{16}	−0.81	5.37×10^{4}	[29]
169.	$HOSO_2 + H = SO_2 + H_2O$	1.0×10^{12}	0.00	0.00	[17]
170.	$HOSO_2 + O = SO_3 + OH$	5.0×10^{12}	0.00	0.00	[17]
171.	$HOSO_2 + OH = SO_3 + H_2O$	1.0×10^{12}	0.00	0.00	[17]
172.	$HOSO_2 + O_2 = SO_3 + HO_2$	7.8×10^{11}	0.00	6.56×10^{2}	[40]
173.	$HOSHO = HOSO + H$	6.4×10^{30}	−5.89	7.38×10^{4}	[17]
174.	$HOSHO = SO + H_2O$	1.2×10^{24}	−3.59	5.95×10^{4}	[17]
175.	$HOSHO + H = HOSO + H_2$	1.0×10^{12}	0.00	0.00	[17]
176.	$HOSHO + O = HOSO + OH$	5.0×10^{12}	0.00	0.00	[17]
177.	$HOSHO + OH = HOSO + H_2O$	1.0×10^{12}	0.00	0.00	[17]
SO_X–NO_X Interactions					
178.	$SO + NO_2 = SO_2 + NO$	8.4×10^{12}	0.00	0.00	[40]
179.	$SO_2 + NO_2 = SO_3 + NO$	6.3×10^{12}	0.00	2.70×10^{4}	[51]
180.	$HSO + NO_2 = HOSO + NO$	5.8×10^{12}	0.00	0.00	[40]

[a] Efficiency factors for the collision partners of this reaction are: $\boldsymbol{\varepsilon}_{H_2O} = 12.0$; $\boldsymbol{\varepsilon}_{H_2} = 2.5$; $\boldsymbol{\varepsilon}_{CO} = 1.9$; $\boldsymbol{\varepsilon}_{CO_2} = 3.8$; $\boldsymbol{\varepsilon}_{Ar} = 0.75$. All other species have efficiencies equal to unity. When a rate constant is declared specifically for argon, the collision efficiency of argon is set equal to zero when determining M for the same reaction.

[b] Fall-off behavior for this reaction is expressed in the form as described in [22].

[c] Reactions 14, 19, and 50 are expressed as the sum of two rate constants.

[d] An efficiency factor for an argon collision partner is specified as $\boldsymbol{\varepsilon}_{Ar} = 0.75$. All other species have efficiencies equal to unity. When a rate constant is declared specifically for argon, the collision efficiency of argon is set equal to zero when determining M for the same reaction.

[e] Efficiency factors for the collision partners of this reaction are $\boldsymbol{\varepsilon}_{H_2O} = 7.5$; $\boldsymbol{\varepsilon}_{Ar} = 0.6$. All other species have efficiencies equal to unity.

[f] Efficiency factors for the collision partners of this reaction are: $\boldsymbol{\varepsilon}_{H_2O} = 12.0$; $\boldsymbol{\varepsilon}_{H_2} = 1.9$; $\boldsymbol{\varepsilon}_{CO} = 1.9$; $\boldsymbol{\varepsilon}_{CO_2} = 3.8$. All other species have efficiencies equal to unity.

[g] Efficiency factors for the collision partners of this reaction are $\boldsymbol{\varepsilon}_{H_2O} = 10.0$; $\boldsymbol{\varepsilon}_{N2} = 1.3$. All other species have efficiencies equal to unity.

between SO_2 and O is in the fall-off regime at pressures above 1 atm. As will be discussed in the following section, we provide an estimate for a high-pressure limit $k_{129,\infty}$ for use with the low-pressure limit $k_{129,0}^{Ar} = 4.0 \times 10^{28}\ T^{-4} \exp(-5250/RT)\ cm^6\ mole^{-2}\ sec^{-1}$ from Troe [30]. The resulting pressure-dependent rate constant $k_{129,eff}$ is an order of magnitude lower than $k_{129,0}[M]$ at pressures approaching 10.0 atm.

In addition to reaction (129), we have modified the pressure-dependencies of $SO_2 + H(+M) = HOSO(+M)$, $SO_2 + H(+M) = HSO_2(+M)$, $SO_2 + OH(+M) = HOSO_2(+M)$, $SO + O(+M) = SO_2(+M)$, and $SO_3 + H + M = HOSO_2 + M$. In general, these latter modifications have a very minor effect on model predictions of the species measured in this study. The low- and high-pressure limits for the recombination of SO_2 and OH via

$$SO_2 + OH\ (+M) = HOSO_2\ (+M) \qquad (130)$$

are taken from Fulle et al. [31] who constructed complete fall-off curves at temperatures between 220 and 400 K. The low-pressure limit for $SO + O(+M) = SO_2(+M)$ is from Astholz et al. [32], and fall-off is calculated using the high-pressure limit and broadening factor as recommended by Cobos et al. [33]. We use a third-order rate constant for the combination of SO_3 and H-atoms rather than the effective second-order rate constant used by Glarborg et al. [17] at atmospheric pressure. The QRRK calculations of Chiang [29] indicate that fall-off in $SO_3 + H(+M) = HOSO_2(+M)$ is not important at the pressures and temperatures of the present study.

The combination of SO_2 and H-atoms to form HSO_2 via

$$SO_2 + H\ (+M) = HSO_2\ (+M) \qquad (165R)$$

has been proposed as an important consumption route for H-atoms affecting the structure of fuel-rich flames [9,34] and inhibiting the hydrogen-oxygen reaction at conditions near the second explosion limit [35]. Recent *ab initio* studies [36,37] indicate the formation of a second, more stable adduct via

$$SO_2 + H\ (+M) = HOSO\ (+M). \qquad (161R)$$

Direct measurements of rate data for reactions (161) and (165) have not been reported and the low- and high-pressure limits used here are from Marshall [38]. The broadening parameters for these reactions are estimates that approximate the fall-off curves generated through RRKM calculations.

Finally, we have modified the rate constant for

$$SO_3 + O = SO_2 + O_2 \qquad (127)$$

based upon the more recent recommendation of Smith et al. [2], which is consistent with the $k_{129,0}^{Ar}$ expression of Troe [30]. The updated k_{127} expression is a factor of three lower than the earlier recommendation of Smith et al. [39] used by Glarborg et al. [17].

EXPERIMENTAL RESULTS AND DISCUSSION

Two experimental approaches were employed in the present study. Reaction profile (time evolution) data were obtained by systematically increasing the distance between the fuel injector and sampling location for mixtures with fixed initial conditions and composition. The species and temperature data from these experiments are compared with model predictions to develop and validate the reaction mechanism. Reactivity trace data were obtained by measuring species data at a single absolute reaction time for varying initial SO_2 or NO mole fractions with all other initial conditions held constant. As mentioned earlier, perturbing processes not simulated properly in the model compromise comparisons made in absolute time. We therefore do not recommend heavily depending upon reactivity trace data to validate the quantitative performance of the reaction mechanism. However, these data provide phenomenological insight into the underlying kinetics over a wide range of initial conditions and thus provide considerable guidance in choosing experimental conditions most appropriate for reaction profile measurements.

Prior to presenting data on the simultaneous effects of SO_2 and NO on moist CO oxidation, we briefly discuss an experiment in which SO_2 is the sole perturbing species. Reactivity trace data for stoichiometric mixtures of 0.5% CO, 0.6% H_2O, 0.25% O_2, 0–1300 ppm SO_2, and N_2 at 3.0 atm and 1020 K are shown in Figure 1. These data were obtained after a nominal residence time of 0.5 seconds, but actual reaction times vary slightly with heat release. The initial temperature is nearly equal to that calculated using the explosion limit criteria $2k_1 = k_{9,eff}$ that demarcates the kinetic regimes of the underlying H_2/O_2 chemistry. As such, the rate of reaction is very sensitive to the loss of radicals and, as seen in Figure 1, even ppm levels of SO_2 dramatically affect the consumption of CO. With increasing SO_2 mole fraction, the catalytic cycle

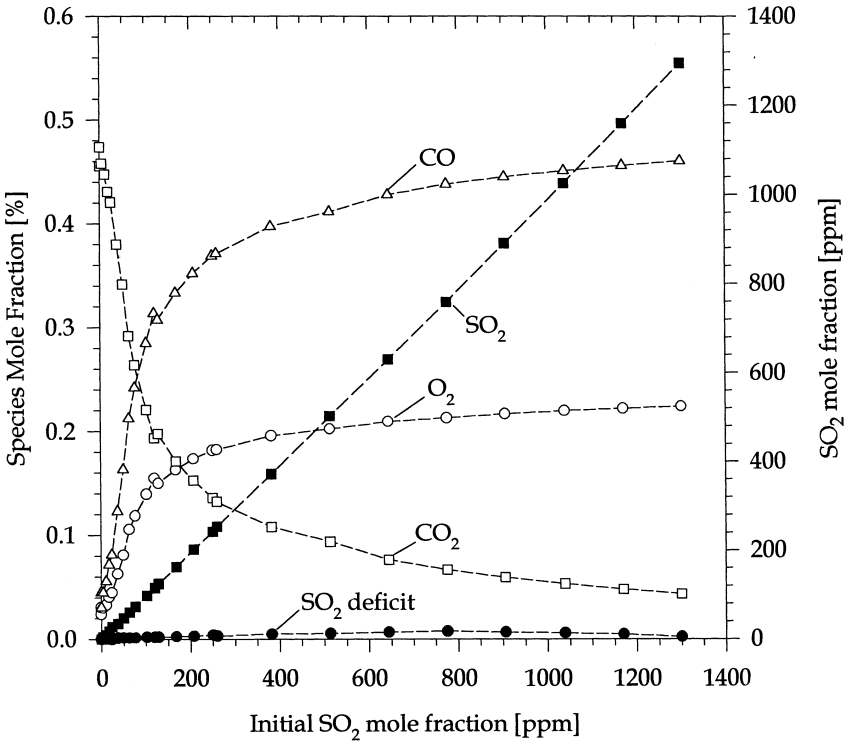

Figure 1 Reactivity trace data for the $CO/H_2O/O_2/SO_2/N_2$ reaction at 3.0 atm and T_{in} = 1020 K with varying SO_2 mole fraction. The nominal residence time is 0.52 seconds; initial mole fractions are given in the text. The dashed lines are not model predictions and are intended only to clarify trends in the experimental data.

$$SO_2 + O\ (+M) = SO_3\ (+M) \qquad (129)$$

$$SO_3 + HO_2 = HOSO_2 + O_2 \qquad (172R)$$

$$HOSO_2\ (+M) = OH + SO_2\ (+M) \qquad (130R)$$

becomes increasingly important and, with reaction (9), yields the net result O + H = OH. In addition to reacting with HO_2, SO_3 reacts with H-atoms via

$$SO_3 + H = SO_2 + OH \qquad (132R)$$

and, to a much lesser extent, with O-atoms,

$$SO_3 + O = SO_2 + O_2. \qquad (127)$$

The sequence of reactions (129) and (132R) also leads to the net result O + H = OH, while reactions (129) and (127) produce the net result O + O = O_2. In each case, the formation and subsequent consumption of SO_3 leads to the loss of radicals that might otherwise lead to chain branching via H + O_2 = OH + O and O + H_2O = OH + OH. The apparent SO_2 deficits (sulfur present as other species) lie between 0–17 ppm, indicating that the fractional conversions of SO_2 to SO_3 are on the order of a few percent.

In addition to reacting with O-atoms, SO_2 reacts with H-atoms via reaction (161) to form HOSO radicals, which, according to model predictions, react predominately with O_2 via

$$HOSO + O_2 = SO_2 + HO_2. \qquad (164)$$

to yield the net result of H + O_2 = HO_2. The extent to which this sequence is inhibiting depends upon the fate of the HO_2 radical. At conditions near the second explosion limit (and in the absence of NO), HO_2 reacts primarily with H, O, and OH radicals. Chain propagation can occur through HO_2 + H = OH + OH, but the terminating reactions HO_2 + H = H_2 + O_2, HO_2 + O = OH + O_2, and HO_2 + OH = H_2O + O_2 lead to an overall inhibiting effect, particularly at fuel-lean conditions where O and OH levels are enhanced relative to H-atoms. SO_2 also combines with OH radicals to form $HOSO_2$ via reaction (130). However, the $HOSO_2$ radical is unstable at these temperatures and rapidly redissociates into SO_2 and OH.

Reactivity trace data showing the simultaneous effects of SO_2 and NO on moist CO oxidation near 950

K at 10.0 atm are provided in Figures 2 and 3. The data in Figure 2 were obtained by varying the initial NO mole fraction with fixed SO_2 and those in Figure 3 show the effects of increasing SO_2 mole fraction with constant NO. The initial conditions of these experiments are such that in the absence of NO, less than 3% of the initial CO is consumed within a residence time of 1.1 seconds. The promoting effects of NO are well established and, in summary, the catalytic cycle consisting of

$$H + O_2 (+M) = HO_2 (+M) \quad (9)$$

$$HO_2 + NO = NO_2 + OH \quad (28)$$

$$NO_2 + H = NO + OH \quad (26)$$

$$CO + OH = CO_2 + H \quad (55)$$

consumes CO while concurrently oxidizing a portion of the NO to NO_2. Initial NO mole fraction permitting, the NO_2 mole fractions attain steady-state levels ($x_{NO_2,SS} = x_{O_2} k_{9,eff}/k_{26}$) that balance the flux of H-atoms through reactions (9) and (26). In large concentrations, however, NO and NO_2 inhibit oxidative processes by catalyzing the recombination of radicals in a manner similar to the processes involving SO_2 and SO_3.

The data in Figure 2 show the characteristic features of these competing effects. CO_2 production increases rapidly when the initial NO mole fraction exceeds $x_{NO_2,SS}$, peaks, and then progressively decreases as inhibiting processes begin to dominate. The addition of SO_2 reduces the observed extent of reaction over the entire range of NO mole fractions, but we note that the inhibition resulting from 463 ppm of SO_2 is small in comparison to that caused by increasing the NO mole fraction from 161 to 420 ppm. In Figure 3, incremental increases in $x_{SO_2,i}$ are seen to only slightly decrease CO_2 production in a mixture with 101 ppm NO. Comparison of these latter data with those in Figure 1 confirms the observation of Glarborg et al. [17] that NO moderates the inhibiting effects of SO_2. Furthermore, although SO_2 and NO_2 react to form NO and SO_3 via

$$NO_2 + SO_2 = NO + SO_3, \quad (179)$$

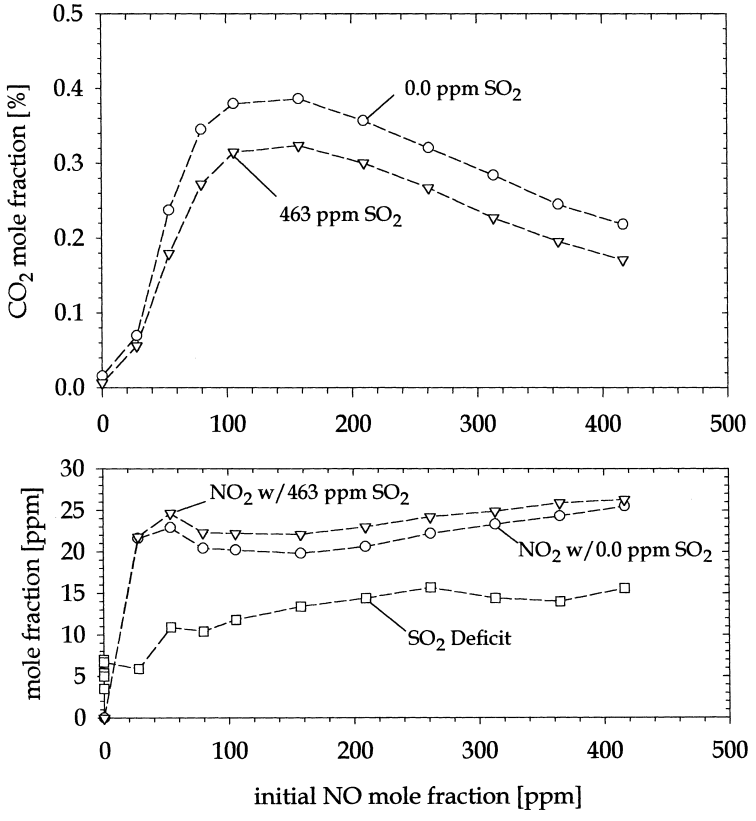

Figure 2 Reactivity trace data for the $CO/H_2O/O_2/NO/SO_2/N_2$ reaction at 10.0 atm and $T_{in} = 954$ K with varying NO mole fraction. The nominal residence time is 1.1 seconds; the initial mole fractions are as follows: $x_{CO} = 0.50\%$; $x_{H_2O} = 0.48\%$; and $x_{O_2} = 0.77\%$. The dashed lines are not model predictions and are intended only to clarify trends in the experimental data.

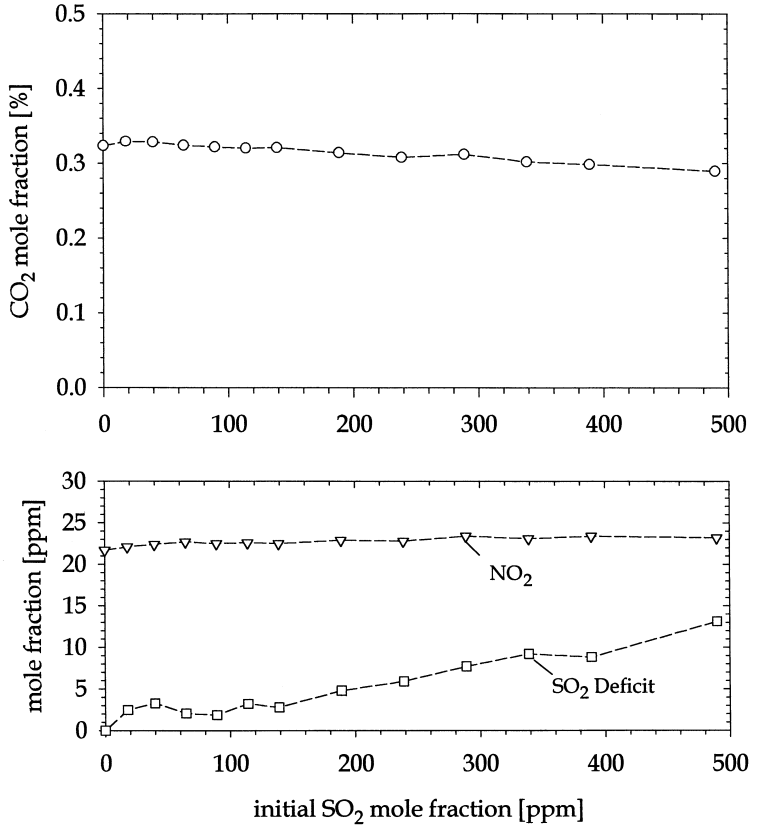

Figure 3 Reactivity trace data for the $CO/H_2O/O_2/SO_2/N_2$ reaction at 10.0 atm and T_{in} = 948 K with varying SO_2 mole fraction. The nominal residence time is 1.1 seconds; the initial mole fractions are as follows: x_{CO} = 0.50%; x_{H_2O} = 0.48%; x_{O_2} = 0.76%; and x_{NO} = 101 ppm. The dashed lines are not model predictions and are intended only to clarify trends in the experimental data.

the addition of SO_2 does not appear to directly affect the fractional conversion of NO to NO_2. The slight increases in NO_2 with increasing SO_2 are consistent with $x_{NO_2,SS} = x_{O_2}k_{9,eff}/k_{26}$ via changes in x_{O_2} accordant with the differing extents of reaction.

In Figure 4, we compare measured CO and NO_2 profiles from $CO/H_2O/O_2/NO/N_2$ reactions at 10.0 atm with and without added SO_2. To facilitate comparisons, the profiles obtained with SO_2 are shifted −0.067 seconds in order to align the times at 50% extent of reaction. These data confirm the trends of the reactivity trace data and clearly show that, at high pressures, the NO-perturbed $CO/H_2O/O_2$ reaction is relatively insensitive to the addition of moderate amounts of SO_2.

Reaction flux analyses reveal that NO diminishes the inhibitory effects of SO_2 through two distinct modes of kinetic coupling via the radical pool. First, the sequence of reactions (161) and (164), leading in turn to HOSO and HO_2, is no longer chain terminating due to the fast reaction between NO and HO_2 (reaction 28). At high pressures, reaction (28) dominates the consumption of HO_2 and the extended sequence of reactions (161), (164), and (28), with the net result H + O_2 + NO = NO_2 + OH, propagates chain carriers. Second, the radical recombination sequences involving NO_X and SO_X species compete for the same radicals. Of particular importance are the additional consumption routes for O-atoms, including

$$NO + O\ (+M) = NO_2\ (+M) \qquad (20)$$

$$NO_2 + O = NO + O_2 \qquad (24)$$

$$NO_2 + O\ (+M) = NO_3\ (+M). \qquad (25)$$

The extent of chain termination initiated by the combination of SO_2 and O-atoms strongly depends on the competition between reaction (129) and reactions (20), (24), and (25). The theoretically derived expression for $k_{129,0}$ is within a factor of two of $k_{20,0}$ and $k_{25,0}$ at the temperatures of this work, but differences in the pressure-dependent rate constants are larger due to differ-

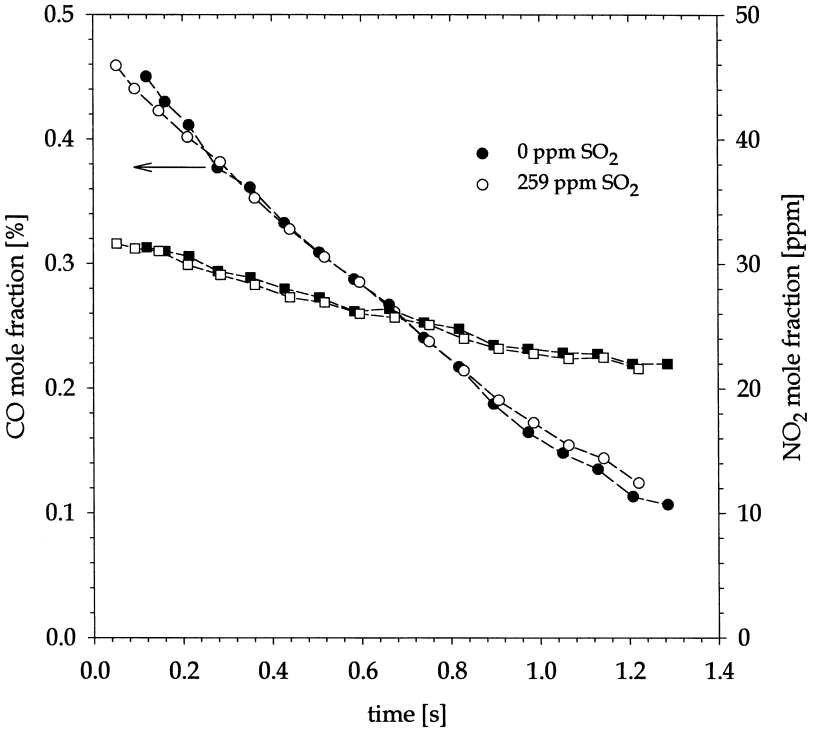

Figure 4 Comparison of reaction profile data for the $CO/H_2O/O_2/NO/N_2$ reaction at 10.0 atm and T_{in} = 955 K with and without 259 ppm of added SO_2. The initial mole fractions are as follows: x_{CO} = 0.52%; x_{H_2O} = 0.48%; x_{O_2} = 0.77%; and x_{NO} = 102 ppm. To facilitate comparisons, the profile obtained with SO_2 is shifted in time as noted in the text. The dashed lines are not model predictions and are intended only to clarify trends in the experimental data.

ing fall-off behavior. Fall-off effects in reactions (20) and (25) produce rather modest (20%) reductions in $k_{20,eff}$ and $k_{25,eff}$ at 1000 K for pressures less than 10.0 atm. The fall-off behavior of reaction (129) is not confirmed as high-pressure data have not been reported; however, Atkinson et al. [40] state that this reaction should be in fall-off at pressures not too far above 1 atm.

Model predictions of the $CO/H_2O/O_2/NO/SO_2/N_2$ reaction are sensitive to the relative rates at which reactions (4), (12), (20), (24), (53), and (129) consume O-atoms. In our initial modeling efforts, we utilized the $k_{129,0}$ expression from Troe [30] without incorporating high-pressure fall-off. An illustrative example of the resulting poor agreement between model predictions and experimental data is shown in Figure 5 for a $CO/H_2O/O_2$ mixture perturbed with 99 ppm of NO and 504 ppm of SO_2 at 3.0 atm and 950 K. The predicted rate of CO consumption is significantly slower than that measured, a discrepancy traceable to the sulfur chemistry as the model predicts very well experimental data from sulfur-free $CO/H_2O/O_2/NO$ mixtures at very similar conditions (see Figs. 17 and 19 of ref. [13]). Reaction flux analyses indicate that over 50% of O-atoms are consumed via $SO_2 + O + M = SO_3 + M$, leading to proportional reductions in the consumption via other routes including, in order of importance, reactions (20), (24), (4), (53), and (12). With the exception of reaction (4), these reactions are chain terminating and model predictions are insensitive to the relative proportioning of the flux through them. However, the reduced flux of O-atoms through $O + H_2O = OH + OH$ significantly reduces the generation of new radicals, thereby slowing the predicted rate of CO consumption.

Feature sensitivity analysis of τ_{5-80}, defined as the time between 5 and 80% of fuel consumption, reveals that reaction (129) is the only reaction from the sulfur submechanism among the 20 most sensitive reactions (the top 12 are shown in Fig. 6). All other reactions involving sulfur-containing species have normalized sensitivity coefficients well below 0.05, a threshold where a factor of 2 change in a rate constant modifies τ_{5-80} by approximately 10%. Although uncertainties remain associated with other reactions in the sulfur submechanism, a large reduction in the effective rate constant for reaction (129) appears to be the only reasonable means to improve the predictive ability of the model with regard to the consumption of CO. This reduction can be achieved through a modification in

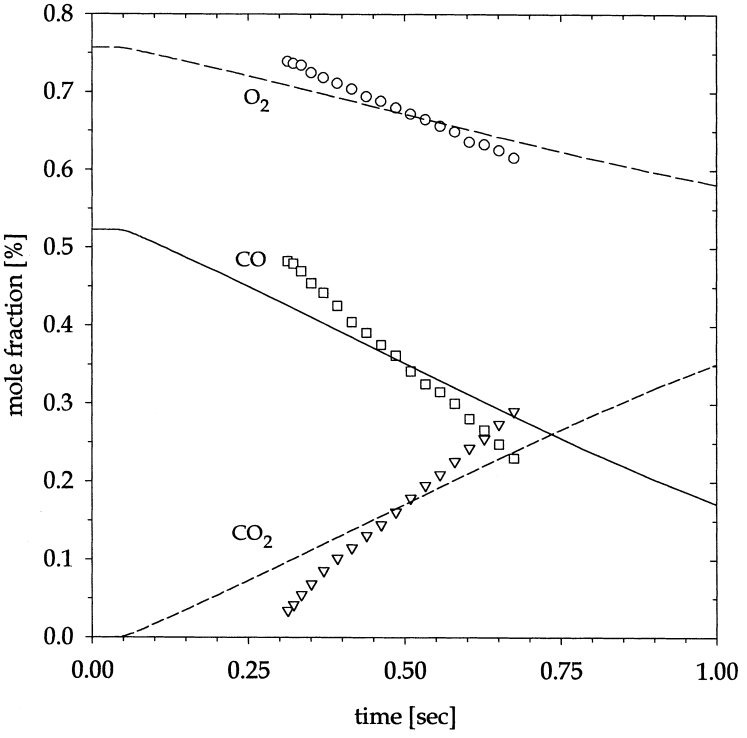

Figure 5 Reaction profile data and initial modeling results for the $CO/H_2O/O_2/NO/SO_2/N_2$ reaction at 3.0 atm and T_{in} = 954 K. Symbols represent the experimental data; the lines are model predictions generated without high-pressure fall-off in $SO_2 + O + M = SO_3 + M$. The initial mole fractions are as follows: x_{CO} = 0.52%; x_{H_2O} = 0.48%; x_{O_2} = 0.76%; x_{NO} = 99 ppm; and x_{SO_2} = 504 ppm. The experimental data are shifted forward in time by 0.352 seconds.

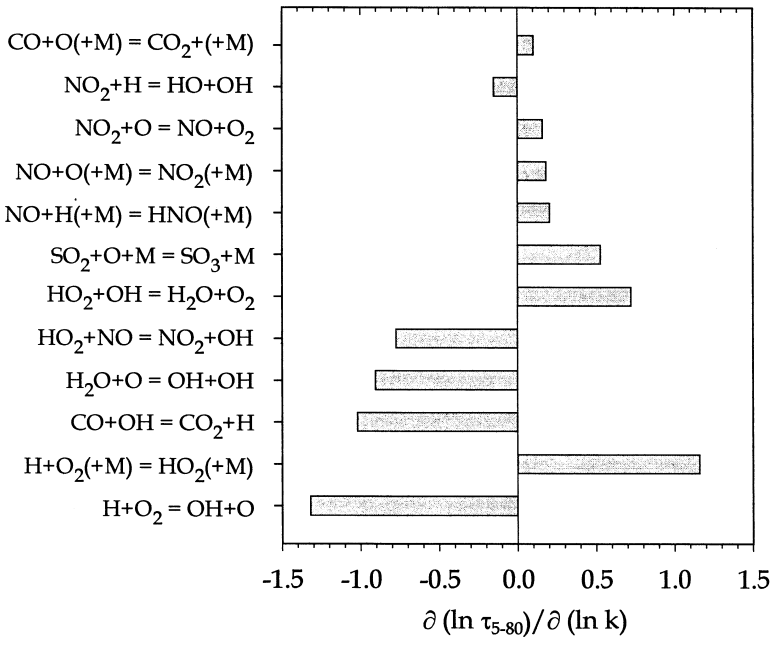

Figure 6 Sensitivity coefficients of the 12 most sensitive rate constants with respect to $\tau_{5\text{-}80}$ as predicted in Figure 5. $\tau_{5\text{-}80}$ is defined as the time duration between 5 and 80% of CO consumption.

the low-pressure limit $k_{129,0}$ or the inclusion of high-pressure fall-off, but the latter approach is clearly favored. If the former approach is chosen, an order of magnitude reduction in $k_{129,0}$ is required to bring the model into agreement with the experimental data. However, an adjustment of this magnitude is inconsistent with available rate data and the theoretical calculations of Troe [30]. On the other hand, a significant reduction in $k_{129,\text{eff}}$ is compatible with the use of a complete pressure-dependent rate constant. Although rate data are not available for the high-pressure limit $k_{129,\infty}$, Astholz et al. [41] and Troe [30] have noted the similarities between the $SO_2 + O = SO_3$ and $CO + O = CO_2$ systems. Both reactions are spin forbidden and have positive temperature dependencies at low temperatures owing to activation barriers on the order of 5 kcal/mol. At high temperatures, these reactions have negative temperature dependencies in accord with reduced rates of collisional stabilization. Troe [42] and Gardiner and Troe [43] provide detailed theoretical and experimental studies of the high-pressure $CO + O = CO_2$ reaction, and Troe's recommendation for $k_{53,\infty}$ forms the basis of our estimate of $k_{129,\infty}$. For modeling purposes, we combine Troe's [30] $SO_2 + O + M = SO_2 + M$ low-pressure limit with our estimate of $k_{129,\infty}$ using a Lindemann fit.

With $k_{129,\infty}$ set equal to $k_{53,\infty}$, $k_{129,\text{eff}}$ is approximately a factor of 20 lower than $k_{129,0}$[M] at 3.0 atm and 950 K. The resulting agreement between predicted and measured CO profile data is very good; however, model predictions become increasingly less sensitive to reaction (129) as it becomes slow in comparison to other reactions. As exemplified in Figure 7, the $CO/H_2O/O_2/NO/SO_2$ profile data are, in fact, more applicable to the determination of an upper limit for $k_{129,\infty}$.

To better estimate $k_{129,\infty}$, we initially set $k_{129,\infty}$ equal to $k_{53,\infty}$ and then adjusted the preexponential constant, $A_{129,\infty}$, as required to fit the consumption of SO_2 in a $N_2O/SO_2/N_2$ mixture at 10.0 atm and 1002 K. The thermal decomposition of N_2O via

$$N_2O\ (+M) = N_2 + O\ (+M) \qquad (47)$$

initiates the reaction by producing O-atoms that subsequently react with SO_2 and N_2O as well as secondary species such as SO_3 and NO (produced via $N_2O + O = NO + NO$). SO_2 profile data (open symbols) are presented in Figure 8 along with model predictions generated using a range of values for $k_{129,\infty}$. These data are considerably more sensitive to $k_{129,\infty}$, and least-squares analyses of the calculated and measured SO_2 profiles indicate an optimal value of 2.78×10^{10} cm^3

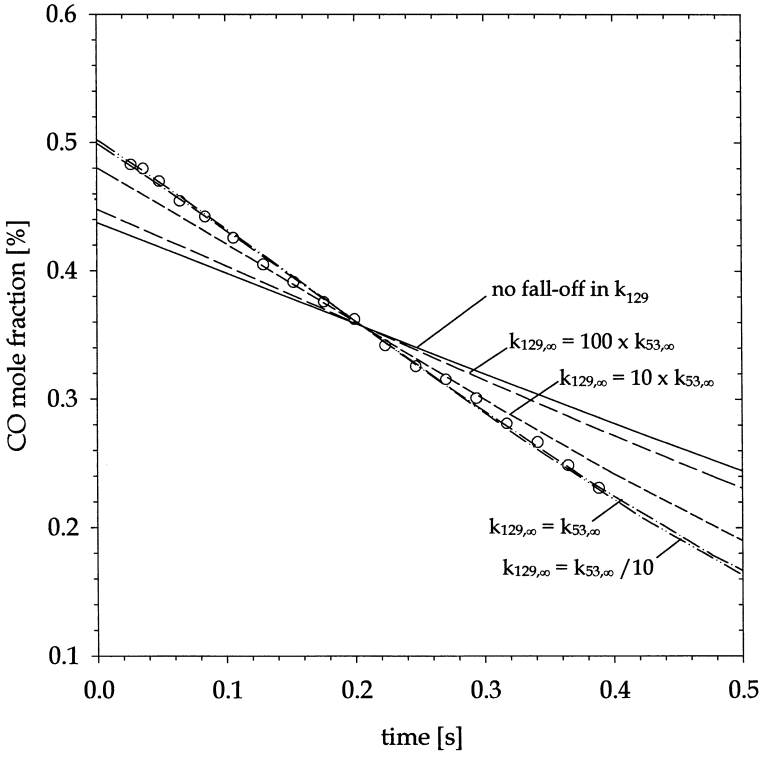

Figure 7 Comparison of the CO profile data from Figure 5 with model predictions generated using various values of $k_{129,\infty}$. For clarity, model predictions are shifted with respect to the experimental data.

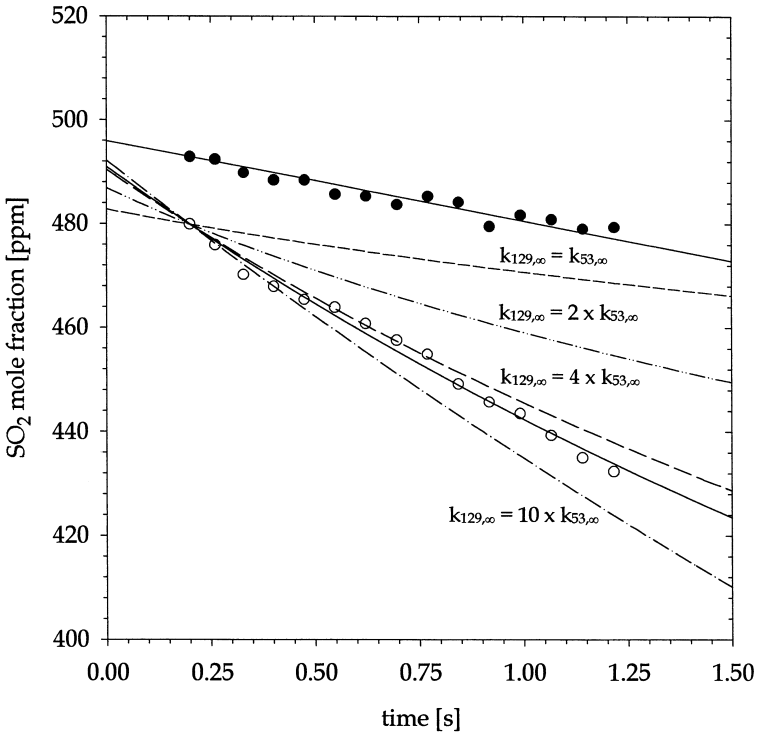

Figure 8 SO_2 profile data and model predictions for the $N_2O/SO_2/N_2$ reaction at 10.0 atm and 1002 K. The open symbols represent data without added NO; the filled symbols represent data with 196 ppm of NO. The initial N_2O and SO_2 mole fractions are 3740 ppm and 506 ppm, respectively. The dashed lines are model predictions generated with values of $k_{129,\infty}$ as indicated; the solid lines are model predictions with the optimized value of $k_{129,\infty} = 9.20 \times 10^{10} \exp(-2380/RT)$ cm^3 mole^{-1} sec^{-1}. Model predictions using the optimized $k_{129,\infty}$ expression are shifted in time by -0.249 and -0.867 seconds, respectively, for the experiments with and without added NO.

mole^{-1} sec^{-1}, or $9.2 \times 10^{10} \exp(-2380/RT)$ cm^3 mole^{-1} sec^{-1} with the assumed temperature dependency. As shown in Figure 9, model predictions are most sensitive to the initiating reaction (47), followed by reactions (129), (127), (49), and (20). We estimate that this determination of $k_{129,\infty}$ is accurate to within a factor of 2, with the primary sources of uncertainty being the respective uncertainties in k_{47} ($\pm$ 31%), k_{127} ($\times/\div$ 3), and k_{49} ($\times/\div$ 4). A more precise fall-off expression can be derived through further investigation of the N_2O/SO_2 system over a range of pressures. However, due to the high activation energy of reaction (47), our studies at temperatures near 1000 K cannot by themselves span a significant range of pressures.

Figure 10 shows the resulting fall-off behavior of $k_{129,\text{eff}}$ at 1000 K in relation to $k_{129,0}$[M] and $k_{129,\infty}$ as well as the rate constants of other important reactions that consume O-atoms in the $CO/H_2O/O_2/NO/SO_2$ system. At 10.0 atm, the complete pressure-dependent expression yields an effective second–order rate constant within 7% of the high-pressure limit and a factor of 14 below $k_{129,0}$[M]. Although extrapolation to lower pressures bears guarded scrutiny, our results indicate that fall-off needs to be considered at pressures at and perhaps even slightly below atmospheric pressure. Also evident in Figure 10 is that with increasing pressure, reaction (129) becomes a less competitive route for O-atoms. At 1 atm, $k_{129,\text{eff}}$ is a factor of 4 lower than $k_{20,\text{eff}}$; at 10 atm, the difference is more than a factor of 20. Comparison of SO_2 profiles obtained using N_2O/SO_2 mixtures with and without added NO confirms the dominance of reaction (20) at high pressures. As seen in Figure 8, the addition of NO significantly slows the consumption of SO_2, indicating clearly that reaction (20) more efficiently scavenges O-atoms at these conditions.

Modification of the reaction mechanism to include fall-off in reaction (129) brings numerical calculations into better agreement with $CO/H_2O/O_2/NO/SO_2$ data obtained over a wide range of pressures. In Figure 11, model predictions are compared to reaction profile data from a series of experiments conducted with approximately the same initial temperature and composition, but with varying pressure. The agreement between predicted and measured rates of CO consumption is excellent and, in line with experimen-

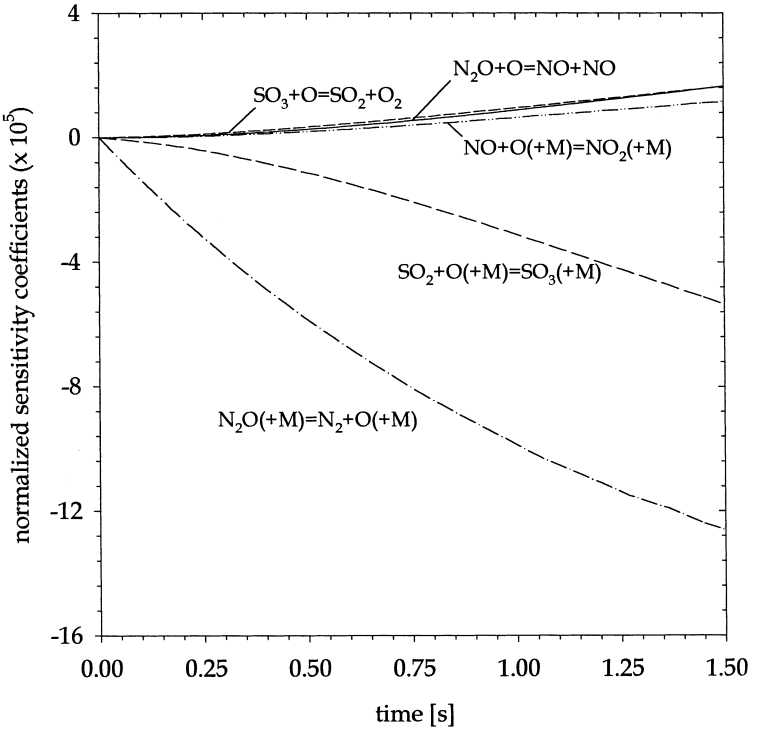

Figure 9 Sensitivity gradients ($S_{ij} = \partial \ln Y_i / \partial \ln k_j$) for the response of the SO_2 mass fraction in the $N_2O/SO_2/N_2$ reaction to variations in the rate constants for the reactions shown. The initial conditions for these calculations are given in Figure 8.

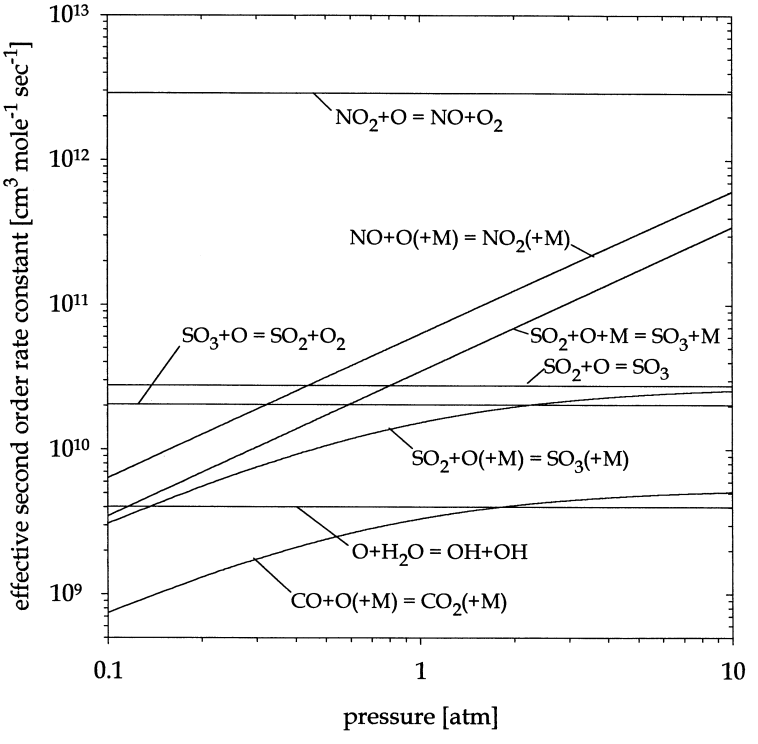

Figure 10 Pressure dependency of the $SO_2 + O(+M) = SO_3(+M)$ reaction at 1000 K in relation to other important reactions that consume O-atoms in the $CO/H_2O/O_2/NO_x/SO_x$ system.

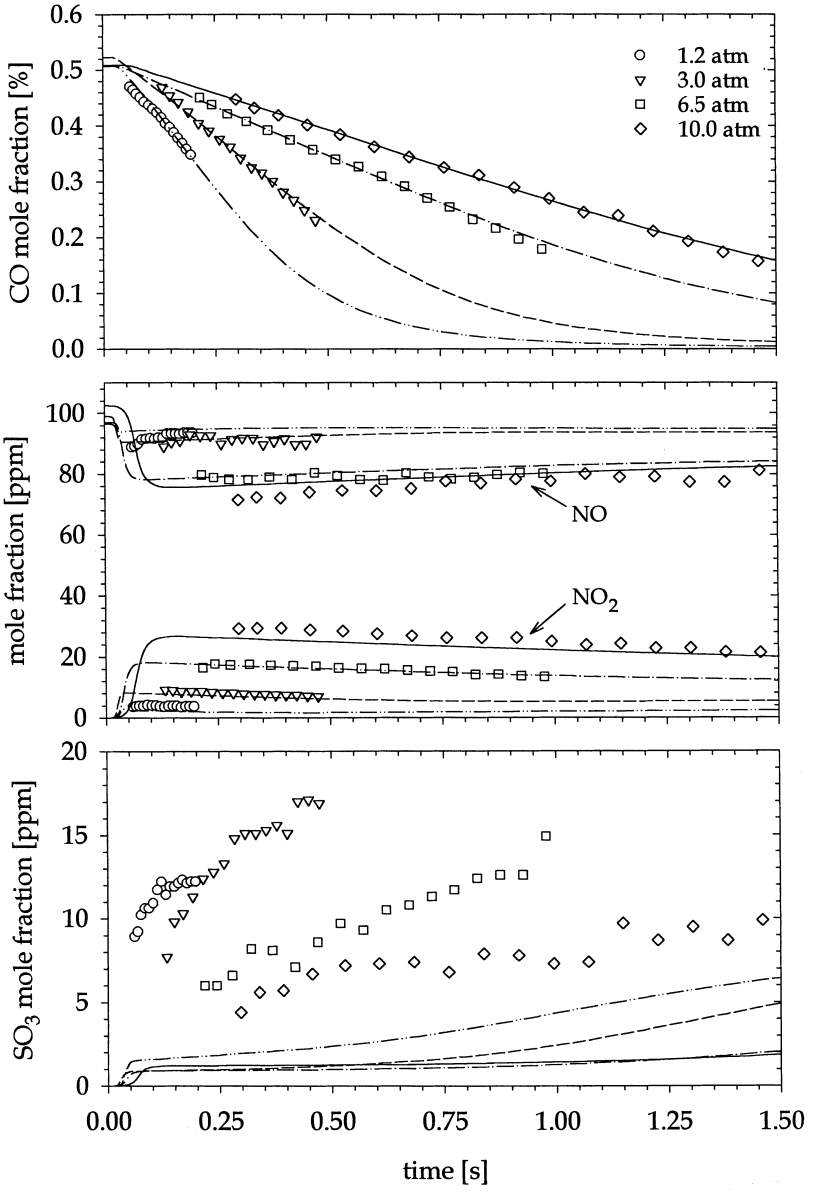

Figure 11 Profile data (symbols) for the $CO/H_2O/O_2/NO/SO_2/N_2$ reaction at pressures ranging from 1.2 to 10.0 atm. Model predictions (lines) were generated using the reaction mechanism given in Table I. Initial temperatures, mole fractions, and timeshifts are as follows: O p = 1.2 atm, T_{in} = 950 K, x_{CO} = 0.51%, x_{O_2} = 0.75%, x_{H_2O} = 0.49%, x_{NO} = 97 ppm, x_{SO_2} = 496 ppm, Δt = 0.041 sec; ∇ p = 3.0 atm, T_{in} = 954 K, x_{CO} = 0.52%, x_{O_2} = 0.76%, x_{H_2O} = 0.48%, x_{NO} = 99 ppm, x_{SO_2} = 504 ppm, Δt = 0.084 sec; $\square$ p = 6.5 atm, T_{in} = 952 K, x_{CO} = 0.52%, x_{O_2} = 0.75%, x_{H_2O} = o,48%, x_{NO} = 97 ppm, x_{SO_2} = 484 ppm, Δt = 0.138 sec; $\diamond$ p = 10.0 atm, T_{in} = 951 K, x_{CO} = 0.51%, x_{O_2} = 0.75%, x_{H_2O} = 0.48%, x_{NO} = 103 ppm, x_{SO_2} = 478 ppm, Δt = 0.178 sec. The experimental measurements of SO_3 are inferred through measurements of $x_{SO_2,in} - x_{SO_2}$.

tal observations, the inhibition resulting from SO_2 interactions with the radical pool is relatively minor at these conditions. Reaction flux analyses of model predictions indicate that reaction (129) accounts for approximately 16% of O-atom consumption at 1.2 atm and less than 8% at 10.0 atm. Without fall-off in reaction (129), these percentages exceed 38% and 61%, respectively. The model also well predicts the NO and NO_2 profiles (the discrepancies at 1.2 atm are discussed later). The fractional conversion of NO to NO_2 is predominantly determined by the flux of H-atoms through reactions (9) and (26), and the good agreement in these profiles indicates that the ratio of $k_{9,eff}/k_{26}$ is well characterized.

However, as seen in the lower part of Figure 11, the model significantly underpredicts the consumption of SO_2 and, presumably, the formation of SO_3. The measured SO_2 deficits range from 1–4% of the initial SO_2 mole fraction, in general agreement with the results of Glarborg et al. [17], who reported fractional conversions of 0–5%. Several studies [44,45,46] have shown that extractive gas sampling can alter NO_X speciation by promoting the conversion of NO to NO_2. To investigate whether similar alterations may occur between SO_2 and SO_3, we numerically simulated the quenching process using an exponentially decaying temperature profile consistent with a 1.5-ms quench time. These calculations indicate that quenching has a considerable effect at conditions where radical levels are of the same order as the stable species of interest (i.e., NO_2 and SO_3). Reaction flux analyses reveal that a catalytic cycle consisting of

$$H + O_2 (+M) = HO_2 (+M) \quad (9)$$

$$NO + HO_2 = NO_2 + OH \quad (28)$$

$$SO_2 + OH (+M) = HOSO_2 (+M) \quad (130)$$

$$HOSO_2 + O_2 = SO_3 + HO_2 \quad (172)$$

$$CO + OH = CO_2 + H \quad (55)$$

simultaneously converts NO to NO_2 and SO_2 to SO_3. The kinetic processes during quenching are distinct from those occurring at higher temperatures in that $HOSO_2$ becomes sufficiently stable such that its reaction with O_2 is preferred over decomposition. Therefore, reactions (130) and (172) now combine to produce rather than consume SO_3. The extent to which the quenching process alters the NO/NO_2 and SO_2/SO_3 ratios depends upon H, O, OH, and HO_2 levels, which, in turn, strongly depend upon the initial mixture temperature, pressure, and stoichiometry. In Figure 12, computed pre- and postquench CO, NO_2, and SO_3 mole fractions are shown for the experimental conditions at 1.2 and 10.0 atm. In both cases, the effect of quenching on the CO profile is insignificant. At 1.2 atm, radical concentrations are equivalent in magnitude to those of NO_2 and SO_3 and, under these circumstances, quenching leads to ppm level increases in both NO_2 and SO_3. The noted discrepancy between predicted and measured NO_X profiles at 1.2 atm is attributed to this effect. Radical levels decrease precipitously with increasing pressure to sub-ppm levels at 3.0 atm and ppb levels at 10.0 atm. As seen in the lower part of Figure 12, the effects of quenching become negligibly small at high pressures.

The measured SO_2 deficits are generally within the absolute uncertainty (±3%) of our FTIR measurements. However, relative differences between data points can be more accurately assessed and we estimate the relative uncertainty in the SO_2 deficits to be ±5 ppm except at 1.2 atm, where quenching effects are most prominent. Thus, the discrepancies in the bottom part of Figure 11 exceed measurement uncertainties. Furthermore, the model does not well predict the trends in the experimental data. In particular, the measured SO_2 deficits generally increase with the extent of reaction, whereas the predicted SO_3 levels are comparatively flat until late reaction times. The data also show a larger pressure dependency than that exhibited by the model. It should be noted here that although fall-off in reaction (129) reduces the predicted SO_3 mole fractions by approximately 50%, the use of $k_{129,0}$ rather than the pressure-dependent rate constant does not resolve these discrepancies.

Given this lack of agreement, conclusions drawn from reaction flux analyses need to be viewed with some skepticism. Nonetheless, these analyses indicate that the formation and consumption of SO_3 is dominated by reactions (129), (132), (172), and (179). The unidirectional fluxes of SO_3 through the forward and reverse directions of reaction (172) are generally much larger than those through reactions (129), (132), and (179). However, reaction (172) is nearly balanced, and when compared on a net basis, the fluxes through each reaction are of the same order. At low pressures, SO_3 is formed primarily through reaction (129), but at higher pressures where O-atoms are predominantly consumed via reactions (20) and (24) and where NO_2 levels are elevated, reaction (179) accounts for a significant fraction of SO_3 production. SO_3 is consumed through reactions (172) and (132), with the former reaction accounting for approximately 75–80% of the net consumption over the range of pressures considered in Figure 11. At lower pressures and/or higher temperatures where $k_1 \gg k_{9,\mathrm{eff}}$, reaction (132) becomes the primary consumption route. The reaction between SO_3 and O-atoms does not appear to contribute significantly to the consumption of SO_3 at the conditions of our experiments.

Sensitivity coefficients for the SO_3 mass fractions at 1.2 and 10.0 atm are shown in Figure 13. In order to highlight sensitivities with respect to the thermochemical data used to derive equilibrium constants, coefficients are given for both forward and reverse rate constants. Reaction numbers followed by the letter "b" correspond to the unidirectional backward reaction. As seen in Figure 13, the predicted SO_3 profiles are sensitive to a large number of reactions that produce and consume radicals. Within the $CO/H_2O/O_2/NO_X$ sub-

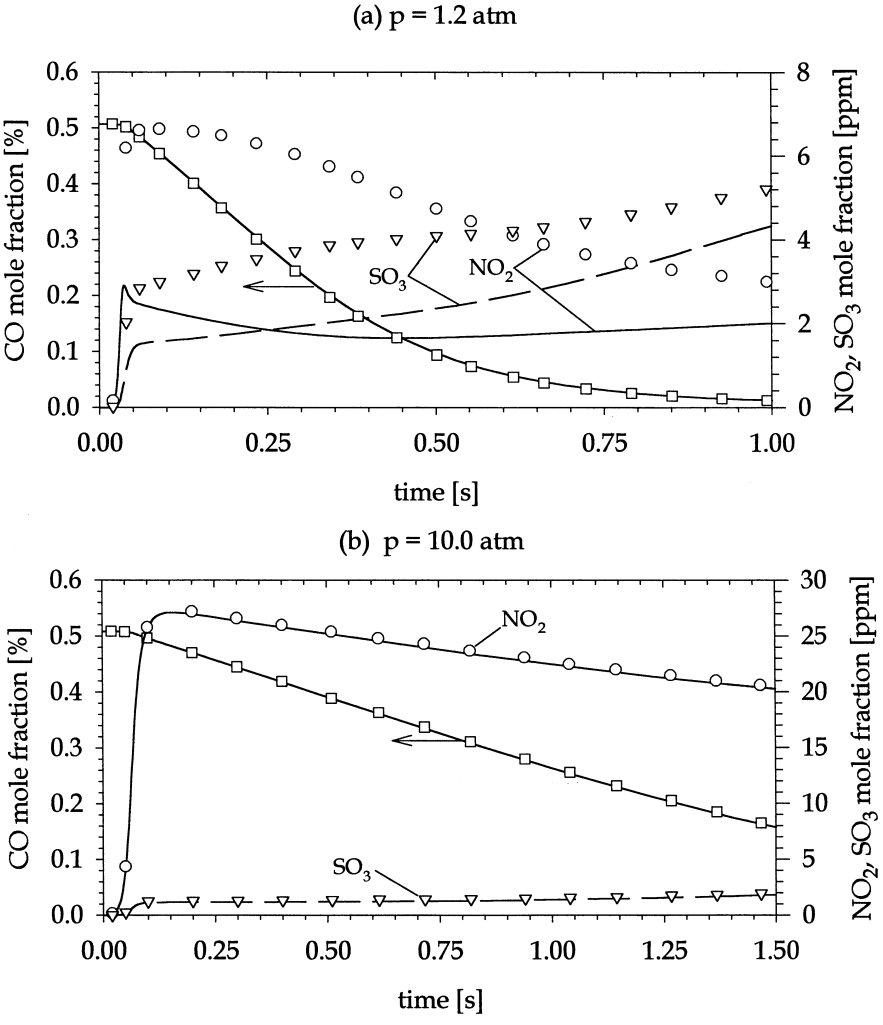

Figure 12 Numerical calculations of the effects of quenching on NO_2 and SO_3 mole fractions at various times in the CO/$H_2O/O_2/NO/SO_2/N_2$ reaction at (a) 1.2 atm and (b) 10.0 atm. Calculations were performed using SENKIN with exponentially decaying temperature profiles to 328 K at constant pressure.

mechanism, the rate constants with the largest sensitivities include k_1, k_4, k_9, k_{28}, and k_{55}. At 1.2 atm, important rate constants from the sulfur submechanism include those for reactions (172b), (129), (132b), (172), (130), and (130b). With increasing pressure, the SO_3 profiles remain sensitive to reactions (172b), (172), (130), and (130b), but the sensitivities for reactions (129) and (132b) decrease and, at 10.0 atm, are over a factor of 10 less than those shown in Figure 13(b). Reaction (130) is microscopically balanced and therefore the important parameter with respect to this reaction is the equilibrium constant, K_{130}. Likewise, the near balance of the fluxes through reactions (172) and (172b) and the sensitivity to k_{172b} indicate a corresponding sensitivity to K_{172}. Both K_{130} and K_{172} are calculated using $\Delta H_f^\circ{}_{HOSO_2}$, for which there is some uncertainty. The value used to generate the results shown in Figure 11 is from Martigan [47], who determined a lower limit of −93.5 kcal/mol in a flash photolysis/resonance fluorescence study of reaction (172). Other literature values include Gleason and Howard's [48] lower limit of −94.5 kcal/mol, Atkinson et al.'s [40] recommendation of −92.0 kcal/mol, and Li and McKee's [49] theoretical calculation of −87.4 kcal/mol.

Within the context of the reaction mechanism provided here, better agreement with the measured SO_2 deficits can be achieved through order of magnitude reductions in the rate constants for both reactions (132b) and (172b). The rate constant for reaction (172b) is calculated using K_{172} and the forward rate constant k_{172} from Gleason and Howard [48], who

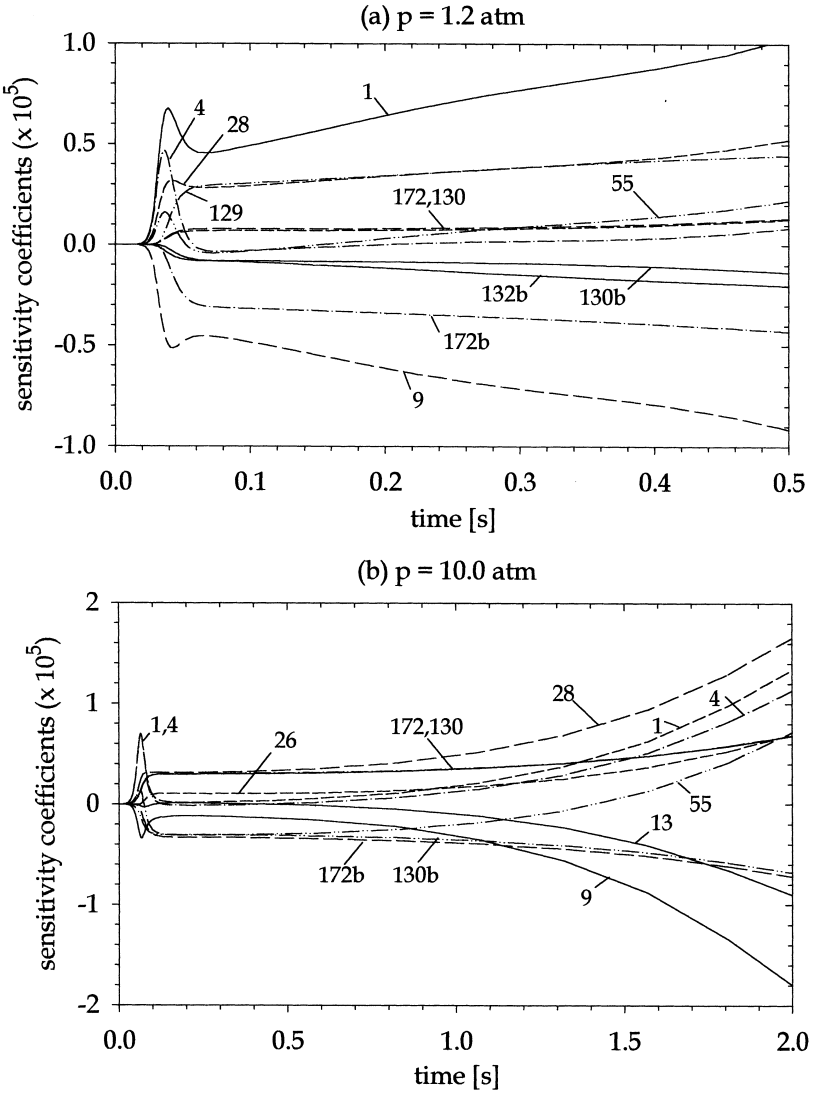

Figure 13 Sensitivity gradients ($S_{ij} = \partial \ln Y_i / \partial \ln k_j$) for the response of the SO_3 mass fraction in the $CO/H_2O/O_2/NO/SO_2/N_2$ reaction at (a) 1.2 atm and (b) 10.0 atm to variations in the rate constants for the reactions shown. The initial conditions for these calculations are given in Figure 11.

measured the loss of $HOSO_2$ radicals using chemical ionization mass spectrometry in a low-pressure discharge flow reactor at temperatures between 287–423 K. These results indicate that the forward reaction $HOSO_2 + O_2 \rightarrow SO_3 + HO_2$ has a small activation energy of 0.66 ± 0.14 kcal/mol that leads to only modest changes in k_{172} upon extrapolation to higher temperatures. No other measurements of the temperature dependency of k_{172} have been reported, but the room temperature data of Gleason and Howard agree with the previous determinations of Martigan [47] and Martin et al. [50] within experimental uncertainty. The adjustment of $\Delta H_f^\circ{}_{HOSO_2}$ to −87.4 kcal/mol reduces k_{172b} by a factor of 20 at 1000 K and, as seen in Figure 14(a), results in approximately a twofold increase in predicted SO_3 mole fractions. With this modification alone, the consumption of SO_3 is predicted to occur primarily through reaction (132b). No rate data have been published for reaction (132b) and the rate constant used here is based upon K_{132} and the semiempirical QRRK estimate of k_{132} by Chiang [29]. Given the lack of experimental data to guide these calculations, there exists some latitude for modification in k_{132}. In Figure 14(b), predicted SO_3 mole fractions generated with $\Delta H_f^\circ{}_{HOSO_2}$ from Li and McKee [49] and a factor of 10 reduction in k_{132} are compared with measured SO_2 deficits. The agreement is much improved and we note that the predicted CO, NO, and NO_2 profiles are

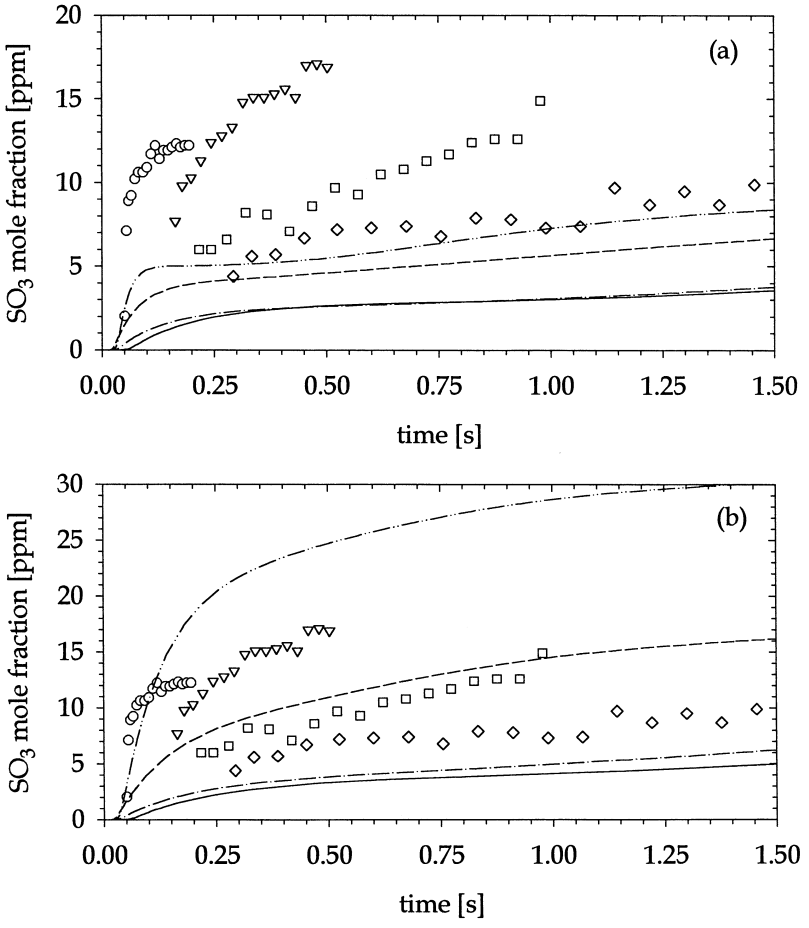

Figure 14 SO_3 profile data compared with model predictions generated with (a) $\Delta H^{\circ}_{fHOSO_2}$ from Li and McKee and (b) $\Delta H^{\circ}_{fHOSO_2}$ from Li and McKee and a factor of 10 reduction in the rate constant for $SO_2 + OH = SO_3 + H$. The symbols, lines, and timeshifts are as defined in Figure 11.

insensitive to these modifications. The remaining discrepancies evident in Figure 14(b) can be reduced further through another 2 kcal/mol increase in $\Delta H_f^{\circ}{}_{HOSO_2}$, a change likely within the uncertainty of Li and McKee's determination.

Finally, the direct reaction between NO_2 and SO_2 is unlikely to be the source of the disparity between measured and predicted SO_2 consumption. As mentioned above, this reaction can be an important source of SO_3 at conditions where the fractional conversion of NO to NO_2 is significant. The rate constant used here is from the static reactor study of Armitage and Cullis [51], who measured the consumption of NO_2 in mixtures of this gas with excess SO_2 at temperatures between 703–1193 K. To verify the accuracy of their determination at our experimental conditions, we obtained reaction profile data using a NO_2/SO_2 mixture at 10.0 atm and 946 K. As shown in Figure 15, these data are well predicted by the model. The slight disparity between the NO and SO_3 mole fractions results from a small contribution to NO production from $NO_2 + NO_2 = NO + NO + O_2$.

CONCLUSIONS

The kinetic coupling associated with moist CO oxidation in the simultaneous presence of NO and SO_2 leads to synergistic effects different from those due to NO or SO_2 alone. Over the range of conditions explored here, the presence of NO significantly reduces the inhibitory nature of SO_2 as its reaction with H-atoms, $SO_2 + H(+M) = HOSO(+M)$, becomes propagating and the combination of SO_2 with O-atoms via $SO_2 + O(+M) = SO_3(+M)$ is slow relative to other O-atom reactions involving NO and NO_2. The data obtained for the consumption of CO indicate that high-pressure fall-off needs to be incorporated into the SO_2

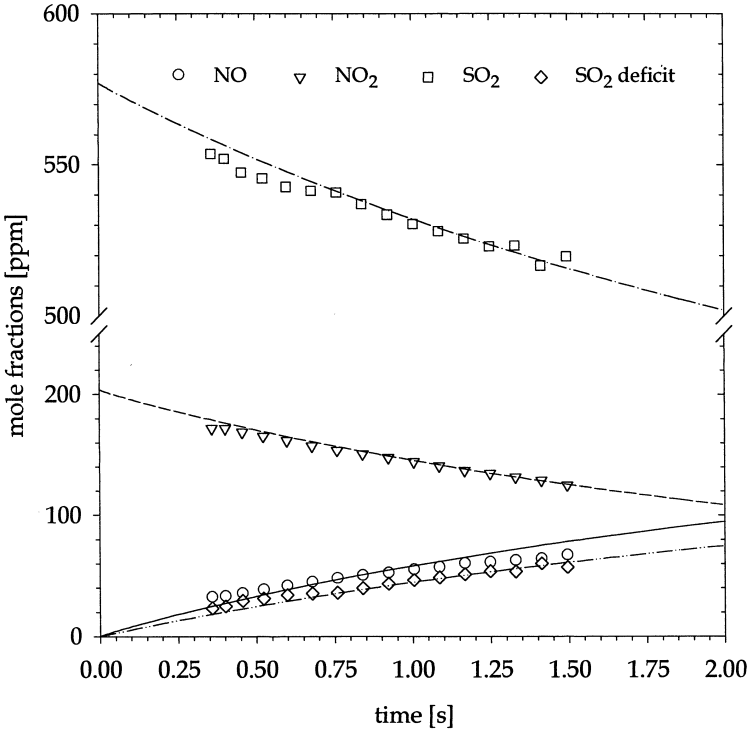

Figure 15 Reaction profile data and model predictions of the NO_2/SO_2 reaction at 10.0 atm and 946 K. The initial mole fractions are 204 ppm and 577 ppm for NO_2 and SO_2, respectively. The experimental data are shifted forward in time by 0.235 seconds.

+ O = SO_3 reaction. Rate data in the high-pressure and fall-off regimes have not previously been reported for this reaction. Kinetic modeling of SO_2 consumption in N_2O/SO_2 mixtures at 10.0 atm and 1000 K provided an estimate for the high-pressure limit, which brings model predictions into good agreement with measured CO profiles. However, predicted SO_3 levels are significantly lower than those suggested by the experimental data. The primary consumption routes for SO_3 are predicted to be $SO_3 + H = SO_2 + OH$ and $SO_3 + HO_2 = HOSO_2 + O_2$. Further study of these reactions is required to confidently predict the fractional conversion of SO_2 to SO_3 in postcombustion gases, but our data support a value of $\Delta H_{f\,HOSO_2}^{\circ}$ consistent with the calculations of Li and McKee [49] as well as a reduction in the rate constant for $SO_3 + H = SO_2 + OH$ as provided here. Our modeling efforts also suggest that ppm levels of radicals can promote the oxidation of SO_2 to SO_3 during sample gas quenching at lower pressures and that the reaction $NO_2 + SO_2 = NO + SO_3$ can account for a significant fraction of SO_3 formation at high pressures.

The perturbation experiments performed in this study expand the experimental database for the development of a comprehensive moist CO oxidation mechanism capable of modeling the postcombustion processing of different residual pollutants that occur in the hot-section and nozzles of gas turbine engines. Similar perturbations also occur in the postcombustion gases from waste material incinerators. With the inclusion of appropriate direct reactions between chlorine- and sulfur-bearing species, the HCl and chloromethane submechanisms of Roesler et al. [11,52] can be added to the present mechanism in order to study the simultaneous interactions of NO_X, SO_2, HCl, CH_3Cl, CH_2Cl_2, $CHCl_3$, and CCl_4.

This work was supported by the NASA Glenn Research Center through Grant No.'s NAG3-1587 and NAG3-2164. The authors also thank Dr. Peter Glarborg, Dr. Jürgen Troe, Dr. Paul Marshall, and Dr. Andrei Kazakov for helpful discussions and Mr. Paul Michniewicz for his assistance in performing the experiments.

BIBLIOGRAPHY

1. Cullis, C. F.; Mulcahy, M. F. R. Combust Flame 1972, 18, 225–292.

2. Smith, O. I.; Wang, S.-N.; Tseregounis, S.; Westbrook, C. K. Combust Sci and Tech 1983, 30, 241–271.
3. Zachariah, M. R.; Smith, O. I. Combust Flame 1987, 69, 125–139.
4. Harris, B. W. ASME Journal of Engineering for Gas Turbines and Power 1990, 112, 585–589.
5. Miake-Lye, R. C.; Anderson, B. E.; Cofer, W. R.; Wallio, H. A.; Nowicki, G. D.; Ballenthin, J. O.; Hunton, D. E.; Knighton, W. B.; Miller, T. M.; Seeley, J. V.; Viggiano, A. A. Geophys Res Lett 1998, 25, 1677–1680.
6. Friedl, R. R., Ed. Atmospheric Effects of Subsonic Aircraft: Interim Assessment Report of the Advanced Subsonic Technology Program 1997; NASA Reference Publication 1400.
7. Brasseur, G. P.; Cox, R. A.; Hauglustaine, D.; Isaksen, I.; Lelieveld, J.; Lister, D. H.; Sausen, R.; Schumann, U.; Wahner, A.; Wiesen, P. European Scientific Assessment of the Atmospheric Effects of Aircraft Emissions, Atmospheric Environment 1998, 32, 2329–2418.
8. Brown, R. C.; Anderson, M. R.; Miake-Lye, R. C.; Kolb, C. E.; Sorokin, A. A.; Buriko, Y. Y. Geophys Res Lett 1998, 23, 3603–3606.
9. Tseregounis, S. I.; Smith, O. I. Twentieth Symposium (International) on Combustion; The Combustion Institute: Pittsburgh, PA, 1984; pp 761–768.
10. Wendt, J. O. L.; Wootan, E. C.; Corley, T. L. Combust Flame 1983, 49, 261–274.
11. Roesler, J. F.; Yetter, R. A.; Dryer, F. L. Combust Flame 1995, 100, 495–504.
12. Glarborg, P.; Kubel, D.; Kristensen, P. G.; Hansen, J.; Dam-Johansen, K. Combust Sci and Tech 1995, 110, 461–485.
13. Mueller, M. A.; Yetter, R. A.; Dryer, F. L. Int J Chem Kinet 1999, 31, 704–724.
14. Hynes, A. J.; Wine, P. H. Combustion Chemistry, 2nd ed.; Gardiner, W. C., Ed.; Springer-Verlag: New York, 1999.
15. Cullis, C. F.; Mulcahy, M. F. R. Combust Flame 1972, 18, 225–292.
16. Frenklach, M.; Lee, J. H.; White, J. N.; Gardiner, W. C. Combust Flame 1981, 41, 1–16.
17. Glarborg, P.; Kubel, D.; Dam-Johansen, K.; Chiang, H.-M.; Bozzelli, J. W. Int J Chem Kinet 1996, 28, 773–790.
18. Yetter, R. A.; Dryer, F. L. Twenty-Fourth Symposium (International) on Combustion; The Combustion Institute: Pittsburgh, PA, 1992; pp 757–767.
19. Scire, J. J.; Yetter, R. A.; Dryer, F. L. In preparation.
20. Allen, M. T.; Yetter, R. A.; Dryer, F. L. Int J Chem Kinet 1995, 27, 883–909.
21. Mueller, M. A.; Kim, T. J.; Yetter, R. A.; Dryer, F. L. Int J Chem Kinet 1995, 31, 113–125.
22. Lutz, A. E.; Kee, R. J.; Miller, J. A. Sandia National Laboratories Report No. SAND87-8248, 1987.
23. Yetter, R. A.; Dryer, F. L.; Rabitz, H. Combust Sci Technol 1997, 79, 129–140.
24. Kim, T. J.; Yetter, R. A.; Dryer, F. L. Twenty-Fifth Symposium (International) on Combustion; The Combustion Institute: Pittsburgh, PA, 1994; pp 759–766.
25. Allen, M. T.; Yetter, R. A.; Dryer, F. L. Combust Flame 1997, 109, 449–470.
26. Tsang, W.; Herron, J. T. J Phys Chem Ref Data 1991, 20, 609–663.
27. Kee, R. J.; Rupley, F. M.; Miller, J. A. Sandia National Laboratories Report No. SAND87-8215, 1987, 1991 update.
28. Hills, A. J.; Howard, C. J. J Chem Phys 1984, 81, 4458–4465.
29. Chiang, H.-M. Ph.D. Thesis, Department of Chemical Engineering, Chemistry, and Environmental Science, New Jersey Institute of Technology: Newark, 1995.
30. Troe, J. Ann Rev Phys Chem 1978, 29, 223–250.
31. Fulle, D.; Hamann, H. F.; Hippler, H. Phys Chem Chem Phys 1999, 1, 2694–2702.
32. Astholz, D. C.; Glänzer, K.; Troe, J. Proceedings of the Eleventh International Symposium on Shock Tubes and Waves, Seattle, WA, 1977, pp 232–237.
33. Cobos, C. J.; Hippler, H.; Troe, J. J Phys Chem 1985, 89, 1778–1783.
34. Fenimore, C. P.; Jones, G. W. J Phys Chem 1965, 69, 3593–3597.
35. Webster, P.; Walsh, A. D. Tenth Symposium (International) on Combustion; The Combustion Institute: Pittsburgh, PA, 1965; pp 463–472.
36. Binns, D.; Marshall, P. J Chem Phys 1991, 95, 4940–4947.
37. Laakso, D.; Smith, C. E.; Goumri, A.; Rocha, J.-D. R.; Marshall, P. Chem Phys Lett 1994, 227, 377–383.
38. Goumri, A.; Rocha, J.-D.; Laasko, D.; Smith, C. E.; Marshall, P. J Phys Chem 1999, 103, 11328–11335.
39. Smith, O. I.; Tseregounis, S.; Wang, S.-N. Int J Chem Kinet 1982, 14, 679–697.
40. Atkinson, R.; Baulch, D. L.; Cox, R. A.; Hampson, R. F.; Kerr, J. A.; Rossi, M. J.; Troe, J. J Phys Chem Ref Data 1997, 26, 521–1011.
41. Astholz, D. C.; Glänzer, K.; Troe, J. J Chem Phys 1979, 70, 2409–2413.
42. Troe, J. Fifteenth Symposium (International) on Combustion; The Combustion Institute: Pittsburgh, PA, 1975; pp 667–680.
43. Gardiner, W.; Troe, J. Combustion Chemistry; Gardiner, W. C., Ed.; Springer-Verlag: New York, 1984; pp 171–196.
44. Johnson, G. M.; Smith, M. Y.; Mulcahy, M. F. R. Seventeenth Symposium (International) on Combustion; The Combustion Institute: Pittsburgh, PA, 1978; pp 647–660.
45. Kramlich, J. C. Combust Sci Tech 1978, 18, 91–104.
46. Allen, J. D. Combust Flame 1975, 24, 133–136.
47. Martigan, J. J. J Phys Chem 1984, 88, 3314–3318.
48. Gleason, J. F.; Howard, C. J. J Phys Chem 1988, 92, 3414–3417.
49. Li, W.-K.; McKee, M. L. J Phys Chem 1997, 101, 9778–9782.
50. Martin, D.; Jourdain, J. L.; Le Bras, G. J Phys Chem 1986, 90, 4143–4147.
51. Armitage, J. W.; Cullis, C. F. Combust Flame 1971, 16, 125–130.

52. Roesler, J. F.; Yetter, R. A.; Dryer, F. L. Combust Sci and Tech 1996. 120, 11–37.
53. Pirraglia, A. N.; Michael, J. V.; Sutherland, J. W.; Klemm, R. B. J Phys Chem 1989, 93, 282–291.
54. Sutherland, J. W.; Michael, J. V.; Pirraglia, A. N.; Nesbitt, F. L.; Klemm, R. B. Twenty-First Symposium (International) on Combustion; The Combustion Institute: Pittsburgh, PA, 1986; pp 929–941.
55. Michael, J. V.; Sutherland, J. W. J Phys Chem 1988, 92, 3853–3857.
56. Sutherland, J. W.; Patterson, P. M.; Klemm, R. B. Twenty-Third Symposium (International) on Combustion; The Combustion Institute: Pittsburgh, PA, 1990; pp 51–57.
57. Tsang, W.; Hampson, R. F. J Phys Chem Ref Data 1986, 15, 1087–1279.
58. Mueller, M. A.; Yetter, R. A.; Dryer, F. L. Twenty-Seventh Symposium (International) on Combustion; The Combustion Institute: Pittsburgh, PA, 1998; pp 177–184.
59. Baulch, D. L.; Drysdale, D. D.; Horne, D. G.; Lloyd, A. C. Evaluated Kinetic Data for High Temperature Reactions, vols. 1 and 2; Butterworths: London, 1973.
60. Cobos, C. J.; Hippler, H.; Troe, J. J Phys Chem 1985, 89, 342–349.
61. Baulch, D. L.; Cobos, C. J.; Cox, R. A.; Frank, P.; Hayman, G.; Just, Th.; Kerr, J. A.; Murrells, T.; Pilling, M. J.; Troe, J.; Walker, R. W.; Warnatz, J. J Phys Chem Ref Data 1994, 23, 847–1033.
62. Hippler, H.; Troe, J.; Willner, J. J Chem Phys 1990, 93, 1755–1760.
63. Warnatz, J. Combustion Chemistry; Gardiner, W. C., Ed.; Springer-Verlag: New York, NY, 1985.
64. Brouwer, L.; Cobos, C. J.; Troe, J.; Dubal, H. R.; Crim, F. F. J Chem Phys 1985, 86, 6171–6182.
65. Hippler, H.; Troe, J. Chem Phys Lett 1992, 192(4), 333–337.
66. Yarwood, G.; Sutherland, J. W.; Wickramaaratchi, M. A.; Klemm, R. B. J Phys Chem 1991, 95, 8771–8775.
67. Hipple, H.; Siefke, M.; Stark, H.; Troe, J. Phys Chem Chem Phys 1999, 1, 57–61.
68. Allen, M. T.; Yetter, R. A.; Dryer, F. L. Combust Flame 1998, 112, 302–311.
69. Fulle, D.; Hamann, H. F.; Hippler, H.; Troe, J. J Chem Phys 1998, 108, 5391–5397.
70. Park, J.; Giles, N. D.; Moore, J.; Lin, M. C. J Phys Chem 1998, A102, 10099–10105.
71. Burkholder, J. B.; Mellouki, A.; Talukdar, R.; Ravishankara, A. R. Int J Chem Kinet 1992, 24, 711–725.
72. Ko, T.; Fontiun, A. J Phys Chem 1991, 95, 3984–3987.
73. Soto, M. R.; Page, M. J Chem Phys 1992, 97, 7287–7296.
74. Soto, M. R.; Page, M. Chem Phys 1996, 153, 415–426.
75. Miller, J. A.; Bowman, C. T. Prog Energy Combust Sci 1989, 15, 287–338.
76. He, Y.; Lin, M. C. Int J Chem Kinet 1992, 24, 743–760.
77. Burkholder, J. B.; Mellouki, A.; Talukdar, R.; Ravishankara, A. R. Int J Chem Kinet 1994, 24, 711–725.
78. Marshall, P.; Ko, T.; Fontijn, A. J Phys Chem 1989, 93, 1922–1927.
79. Miller, J. A.; Melius, C. F.; Durant, J. L. Unpublished work: personal communication with J. A. M., 1994.
80. Hanson, R. K.; Salimian, S. Combustion Chemistry; Gardiner, W. C., Ed.; Springer-Verlag: New York, NY, 1985.
81. Westmoreland, P. R.; Howard, J. B.; Longwell, J. P.; Dean, A. M. AIChE J 1986, 32, 1971–1979.
82. Troe, J. Fifteenth Symposium (International) on Combustion; The Combustion Institute: Pittsburgh, PA, 1975; pp 667–680.
83. Yu, C.-L.; Wang, C.; Frenklach, M. Temperature and Pressure Dependence of Reaction CO+OH: Application of Unimolecular Theory with Solution Mapping Method; Eastern States Meeting of The Combustion Institute, Ithaca, NY, 1991.
84. Loirat, H.; Caralp, F.; Destriau, M. J Phys Chem 1983, 87, 2455–2457.
85. Timonen, R. S.; Ratajczak, E.; Gutman, D. J Phys Chem 1987, 91, 5325–5332.
86. Timonen, R. S.; Ratajczak, E.; Gutman, D. J Phys Chem 1988, 92, 651–655.
87. Timonen, R. S.; Ratajczak, E.; Gutman, D. J. Phys Chem 1987, 91, 692–694.
88. Lin, C.-Y.; Wang, H.-T.; Lin, M. C.; Melius, C. F. Int J Chem Kinet, 1990, 22, 455–482.
89. Chung, K.; Calvert, J. G.; Bottenheim, J. W. Int J Chem Kinet, 1975, 7, 161–182.
90. Bauer, S. H.; Jeffers, P.; Lifshitz, A.; Yadava, B. P. Thirteenth Symposium (International) on Combustionl The Combustion Institute: Pittsburgh, PA, 1971; pp 417–425.
91. Plach, H. J.; Troe, J. Int J Chem Kinet 1984, 16, 1531–1542.
92. DeMore, W. B.; Golden, D. M.; Hampson, R. F.; Howard, C. J.; Kurylo, M. J.; Molina, M. J.; Ravishankara, A. R.; Sanders, S. P. JPL Publications 1987, 1, 87–41.
93. Woiki, D.; Roth, P. Int J Chem Kinet, 1995, 27, 59–71.
94. Martinez, R. I.; Herron, J. T. Int J Chem Kinet 1983, 15, 1127–1132.